THE JOURNAL OF BIOLOGICAL CHEMISTRY
Vol. 280, No. 1, Issue of January 7, pp. 847–851, 2005
Printed in U.S.A.

Involvement of Endoplasmic Reticulum Stress in Insulin Resistance and Diabetes*

Received for publication, October 19, 2004
Published, JBC Papers in Press, October 27, 2004, DOI 10.1074/jbc.M411860200

Yoshihisa Nakatani‡§, Hideaki Kaneto‡§¶, Dan Kawamori‡, Kazutomi Yoshiuchi‡, Masahiro Hatazaki‡, Taka-aki Matsuoka‡, Kentaro Ozawa‖, Satoshi Ogawa‖, Masatsugu Hori‡, Yoshimitsu Yamasaki‡, and Munehide Matsuhisa‡

From the ‡Department of Internal Medicine and Therapeutics, Osaka University Graduate School of Medicine, 2-2 Yamadaoka, Suita, Osaka 565-0871 and the ‖Department of Neuroanatomy, Kanazawa University Medical School, 13-1 Takara-machi, Kanazawa, Ishikawa 920-8640, Japan

Type 2 diabetes is one of the most prevalent and serious metabolic diseases in the world, and insulin resistance and pancreatic β-cell dysfunction are the hallmarks of the disease. In this study, we have shown that endoplasmic reticulum (ER) stress, which is provoked under diabetic conditions, plays a crucial role in the insulin resistance found in diabetes by modifying the expression of oxygen-regulated protein 150 (ORP150), a molecular chaperone that protects cells from ER stress. Sense ORP overexpression in the liver of obese diabetic mice significantly improved insulin resistance and markedly ameliorated glucose tolerance. Conversely, expression of antisense ORP150 in the liver of normal mice decreased insulin sensitivity. The phosphorylation state of IRS-1 and Akt, which are key molecules for insulin signaling, and the expression levels of phosphoenolpyruvate carboxykinase and glucose-6-phosphatase, key enzymes of gluconeogenesis, were also altered by ORP150 overexpression. This is the first report showing that ER stress plays a crucial role in the insulin resistance found in diabetes and thus could be a potential therapeutic target for diabetes.

Type 2 diabetes is one of the most prevalent and serious metabolic diseases in the world, and insulin resistance and pancreatic β-cell dysfunction are the hallmarks of the disease (1, 2). Normal β-cells can compensate for insulin resistance by increasing insulin secretion, but insufficient compensation leads to the onset of glucose intolerance. Once hyperglycemia becomes apparent, insulin resistance is further increased and β-cell function progressively deteriorates. The significance of hyperglycemia as a direct cause of these phenomena has been called "glucose toxicity" (3, 4).

The endoplasmic reticulum (ER)[1] is an organelle that synthesizes various secretory and membrane proteins. These proteins are correctly folded and assembled by chaperones in the ER. During stressful conditions, such as an increase in the misfolded protein level, the chaperons become overloaded and the ER fails to fold and export newly synthesized proteins, leading to ER stress (5–9). We hypothesized that the ER stress provoked in diabetes is involved in various phenomena found in the disease. It has indeed previously been shown that ER stress is involved in pancreatic β-cell dysfunction (10–14). Oxygen-regulated protein 150 (ORP150), a molecular chaperone found in the ER, has been shown to protect cells from ER stress (15, 16). Here we report that ORP150 overexpression markedly improves insulin resistance and ameliorates glucose tolerance in diabetic animals, indicating that ER stress plays a crucial role in insulin resistance and could be a potential therapeutic target for diabetes.

MATERIALS AND METHODS

Preparation of Recombinant Adenoviruses—Recombinant adenoviruses expressing sense ORP (Ad-S-ORP) and antisense ORP (Ad-AS-ORP) were prepared, and the adenovirus titers were increased up to 1×10^8 pfu/ml in the 293 cells. Adenovirus titers were further increased up to 1×10^{10} pfu/ml using Adeno-X™ virus purification kit (Clontech). Control adenovirus expressing green fluorescent protein (Ad-GFP) was also prepared in the same manner. Virus titers were estimated using an Adeno-X™ titer kit (Clontech).

Animals and Administration of Recombinant Adenoviruses—Male C57BL6 and C57BL/KsJ-db/db mice were purchased from Japan SLC. Mice (8 weeks old) were injected with Ad-S-ORP, Ad-AS-ORP, or Ad-GFP (1×10^{10} pfu/ml for Ad-S-ORP and 2×10^9 pfu/ml for Ad-AS-ORP) from the cervical vein. After adenovirus injection, blood glucose levels were measured regularly with a portable glucose meter (Glu-test Sensor; Sanwa) after tail snipping. For measurement of serum insulin levels, blood samples of mice after a 6-h fast were collected into heparinized capillary tubes and serum insulin levels were determined with an insulin-EIA test kit (Glazyme).

Glucose Tolerance Tests—After a 6-h fast, mice were injected intraperitoneally with glucose (2.0 g/kg body weight). Blood samples were taken at various time points (0–120 min), and blood glucose levels and serum insulin levels were determined as described above.

Insulin Tolerance Tests—After a 6-h fast, mice were injected intraperitoneally with insulin (2.0 units/kg for C57BL-KsJ-db/db mice). Blood samples were taken at various time points (0–90 min), and blood glucose levels were measured as described above.

Euglycemic Hyperinsulinemic Clamp—Fourteen days before the clamp study, Ad-S-ORP (1×10^{10} pfu/ml) or Ad-AS-ORP (2×10^9 pfu/ml) was injected from the left jugular vein. Three days before the clamp study, a silicon catheter (Phicon tube; Fuji-Systems) was inserted into the right jugular vein under general anesthesia with sodium pentobarbital. The catheter, which is required for infusion in the clamp study, was exteriorized at the back of the neck through a subcutaneous tunnel and filled with heparinized saline (200 units/ml). Clamp studies were performed on mice under conscious and unstressed conditions after a 6-h fast. A euglycemic hyperinsulinemic clamp with a tracer dilution method was applied to determine peripheral glucose uptake and endogenous glucose production. Experiments consisted of a 120-min euglycemic hyperinsulinemic clamp period (15 pmol/kg/min of regular human insulin for C57BL6 mice, 27 pmol/kg/min for C57BL/KsJ-

* This work was supported in part by grants from the Ministry of Education of Japan (to Y. Y.). The costs of publication of this article were defrayed in part by the payment of page charges. This article must therefore be hereby marked "*advertisement*" in accordance with 18 U.S.C. Section 1734 solely to indicate this fact.

§ Both authors contributed equally to this work.
¶ To whom correspondence should be addressed. Tel.: 81-6-6879-3633; Fax: 81-6-6879-3639; E-mail: kaneto@medone.med.osaka-u.ac.jp.

[1] The abbreviations used are: ER, endoplasmic reticulum; ORP150, oxygen-regulated protein 150; Ad-S-ORP, adenovirus expressing sense ORP; Ad-AS-ORP, adenovirus expressing antisense ORP; pfu, plaque-forming unit; GFP, green fluorescent protein; HGP, hepatic glucose production; MOPS, 4-morpholinepropanesulfonic acid.

db/db mice during the 120-min clamp period). During this period, blood glucose levels were monitored every 5 min and the rate of 50% glucose containing 10% [6,6-$^2H_2$]glucose infusion into the jugular vein was adjusted to maintain blood glucose concentrations at 120 ± 10 mg/dl.

Measurement of Endogenous Hepatic Glucose (HGP) Production by Stable Isotope-labeled Glucose Enrichment—To estimate HGP, stable isotope-labeled glucose enrichment was determined. Blood samples were taken at 90, 105, and 120 min, and 20 μl of each plasma sample were deproteinized with 60 μl of 99.5% ethanol. The supernatant was evaporated, and the residue was derivatized by the following procedure. First, 7.5 μl of MBTFA (*N*-methyl-bis (trifluoroacetamide); Pierce) and 7.5 μl of pyridine were added to the residue, and the mixture was heated for 1 h at 60 °C. The reaction product (1 μl) containing trifluoroacetylated glucose was then analyzed by gas chromatography and mass spectrometry (Model TSQ-700; Finningan-MAT) with a silicon S.E.-30 capillary column (30 m × 0.25 mm; Gasukuro Kogyo). The trifluoroacetyl derivative of glucose was separated from the other compounds by gas chromatography and was analyzed by electron impact mass spectrometry at 70 eV. The fragment ion peaks of unlabeled and [6,6-$^2H_2$]glucose were measured at a mass/electrical charge of 319 and 321, respectively.

Western Blot Analysis and Immunoprecipitation—Whole cell extracts obtained from liver were fractionated by 10% SDS-PAGE and transferred to reinforced cellulose nitrate membrane (Optitran BA-S85; Schleicher & Schuell). After blocking, the membranes were incubated at 4 °C overnight in TBS buffer (50 mM Tris-HCl, 150 mM NaCl) containing a 1:1000 dilution of rabbit anti-IRS-1 antibody (Upstate Biotechnology), anti-Akt, and anti-Akt-pSer473 antibody (Cell Signaling) and then incubated for 1 h at room temperature in TBS containing a 1:1000 dilution of anti-rabbit IgG antibody coupled to horseradish peroxidase (Bio-Rad). In addition, expression of the tyrosine-phosphorylated form of IRS-1 was examined by immunoprecipitation using anti-IRS-1 and anti-phosphotyrosine antibody (Upstate Biotechnology). Immunoreactive bands were visualized by incubation with LumiGLO (Cell Signaling) and exposed to light-sensitive film.

Northern Blot Analysis—Ten micrograms of total RNA isolated from freeze-clamped liver tissues were electrophoresed on 1.0% formaldehyde-denatured agarose gel in 1 × MOPS running buffer and then transferred overnight to a Hybond-N$^+$ membrane (Amersham Biosciences). The phosphoenolpyruvate carboxykinase and glucose-6-phosphatase cDNA probes were labeled with [α-^{32}P]dCTP using a Rediprime labeling system kit (Amersham Biosciences). After overnight hybridization with a ^{32}P-labeled probe at 42 °C, the membranes were washed in 2 × SSPE (saline/sodium phosphate/EDTA), 0.1% SDS at 42 °C. The probed membranes were exposed to an imaging plate, BAS-MS 2040 (Fujifilm), and the hybridization intensity was quantified using a BAS2500 system (Fujifilm).

Statistical Analysis—Results are expressed as mean ± S.E. Differences between groups were examined for statistical significance using the Student's *t* test or analysis of variance with the Fisher's test.

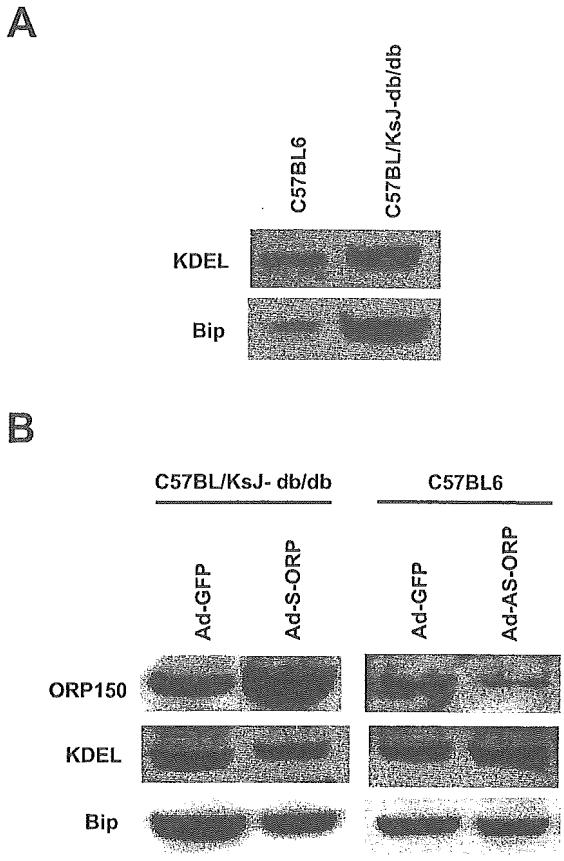

FIG. 1. **Induction of ER stress under diabetic conditions and reduction of ER stress by adenoviral sense ORP overexpression.** *A*, induction of ER stress under diabetic conditions. Expression levels of KDEL and Bip, ER stress markers, in 10-week-old obese diabetic C57BL/KsJ-db/db and non-diabetic C57BL6 mice were examined by Western blot analysis. Similar results were obtained in three independent experiments. *B*, reduction of ER stress by adenoviral sense ORP overexpression. C57BL/KsJ-db/db mice were treated with Ad-S-ORP or Ad-GFP, and C57BL6 mice were treated with Ad-AS-ORP or Ad-GFP. Two weeks after the adenovirus injection, expression levels of KDEL and Bip were examined by Western blot analysis. Similar results were obtained in three independent experiments.

RESULTS AND DISCUSSION

ORP150 Overexpression in the Liver Markedly Reduces Insulin Resistance and Ameliorates Glucose Tolerance in Obese Diabetic C57BL/KsJ-db/db Mice—First, to examine whether ER stress is increased in the liver under diabetic conditions, we evaluated ER stress levels in the livers of 10-week-old obese diabetic C57BL/KsJ-db/db mice. Expression levels of KDEL and Bip, both of which are ER stress markers, were much higher in the obese diabetic mice compared with 10-week-old non-diabetic C57BL6 mice (Fig. 1*A*), indicating that ER stress is actually increased under diabetic conditions. To examine the effect of sense ORP150 overexpression on insulin resistance and diabetes, we prepared sense ORP150 expressing Ad-S-ORP (1×10^{10} pfu/ml) and a GFP-expressing control adenovirus (Ad-GFP) and delivered each adenovirus to 8-week-old C57BL/KsJ-db/db obese diabetic mice from the cervical vein. By Western blot analysis we confirmed an increase in ORP150 expression in the liver upon adenovirus injection (Fig. 1*B*), but not in other tissues such as muscle and adipose tissue (data not shown). In addition, expression levels of KDEL (GRP78/94) and Bip (GRP78) in Ad-S-ORP-treated mice were lower compared with those in Ad-GFP-treated db/db mice, indicating that ORP150 is actually acting to decrease ER stress in the liver (Fig. 1*B*). There was no difference in body weight and food intake between Ad-S-ORP-treated and Ad-GFP-treated-db/db mice (data not shown). When C57BL/KsJ-db/db mice were treated with Ad-S-ORP, nonfasting blood glucose levels were markedly reduced (Fig. 2*A*), whereas no such effects were observed in Ad-GFP-treated mice (Fig. 2*A*) or in C57BL6 mice treated with Ad-S-ORP (data not shown). Fasting blood glucose concentrations (after a 6-h fast) were also significantly lower in Ad-S-ORP-treated mice compared with Ad-GFP-treated mice, although there was no difference in plasma insulin concentrations between the two groups (Fig. 2*B*). To examine the effects of ORP150 overexpression in the liver on insulin resistance, we performed the intraperitoneal insulin tolerance test. The hypoglycemic response to insulin was larger in Ad-S-ORP-treated C57BL/KsJ-db/db mice than in Ad-GFP-treated mice (Fig. 2*C*). To investigate this point further, we performed the euglycemic hyperinsulinemic clamp test. Clamp studies were performed on mice under conscious and unstressed conditions after a 6-h fast. Experiments consisted of a 120-min euglycemic hyperinsulinemic clamp period (15 pmol/kg/min of regular human insulin for C57BL6 mice, 27 pmol/kg/min for C57BL/KsJ-db/db mice). Blood glucose levels were monitored every 5 min, and the rate of infusion of a 50% glucose solution containing 20% [6,6-$^2H_2$]glucose into the jugular vein was adjusted to maintain

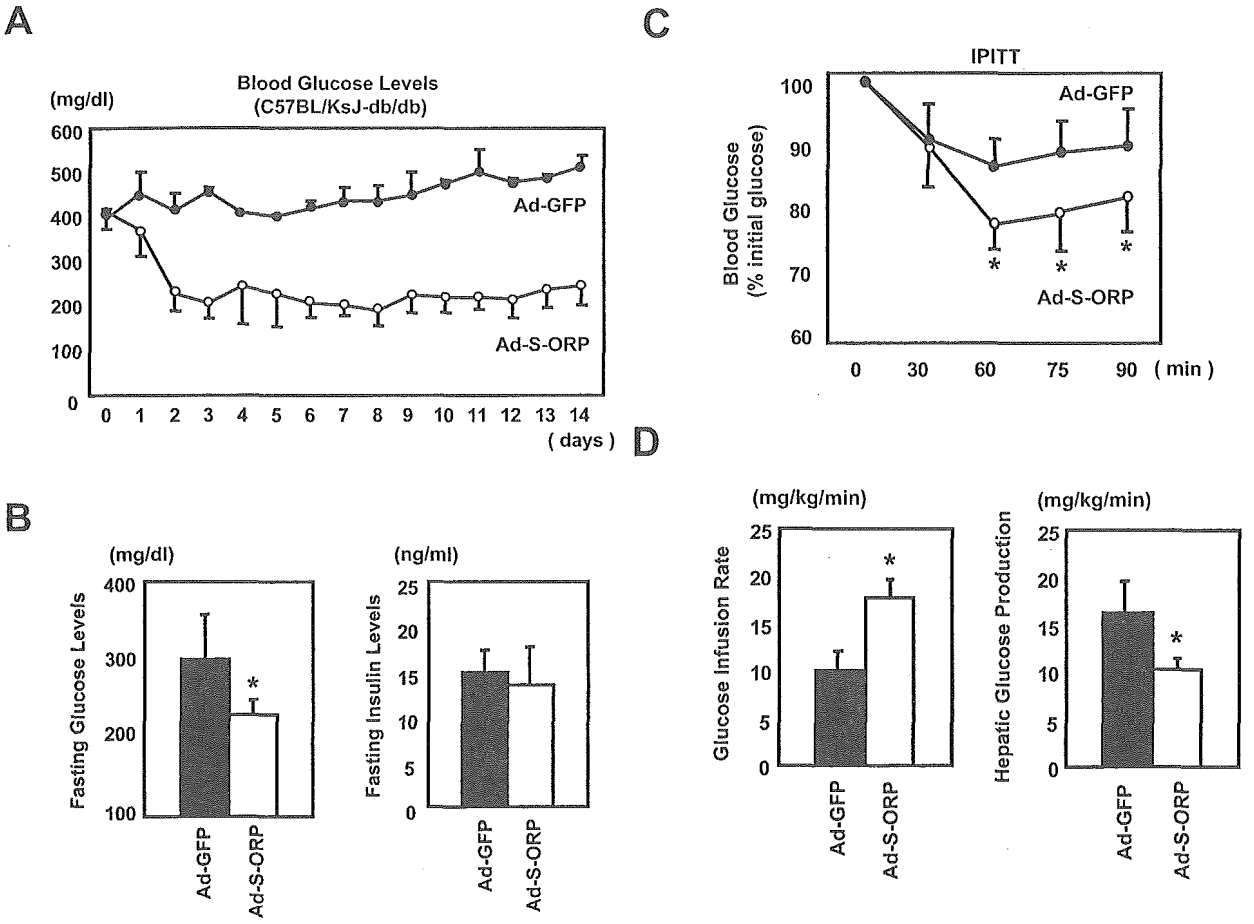

FIG. 2. **Effects of adenoviral sense ORP overexpression in the liver on insulin resistance and glucose tolerance in C57BL/KsJ-db/db mice.** *A*, nonfasting blood glucose levels in C57BL/KsJ-db/db mice treated with Ad-S-ORP or Ad-GFP ($n = 6$). *B*, fasting blood glucose and serum insulin levels in C57BL/KsJ-db/db mice 2 weeks after injection with Ad-S-ORP or Ad-GFP (*, $p < 0.05$, $n = 6$). *C*, insulin resistance in C57BL/KsJ-db/db mice treated with Ad-S-ORP or Ad-GFP. Two weeks after the adenovirus injection, intraperitoneal insulin tolerance tests (*IPITT*) were performed. After a 6-h fast, insulin was injected intraperitoneally at a dose of 2.0 units/kg body weight, and blood glucose levels were measured (*, $p < 0.05$, $n = 6$). *D*, glucose infusion rate and endogenous hepatic glucose production in C57BL/KsJ-db/db mice treated with Ad-S-ORP or Ad-GFP. Two weeks after the adenovirus injection, glucose infusion rate and hepatic glucose production were estimated by a euglycemic hyperinsulinemic clamp test (*, $p < 0.05$, $n = 6$).

blood glucose concentrations at 110 ± 10 mg/dl. The glucose infusion rates (GIR) of Ad-S-ORP-treated mice were significantly higher compared with Ad-GFP-treated mice (17.9 ± 3.7 *versus* 10.0 ± 2.8 mg/kg/min, $p < 0.05$) (Fig. 2*D*), indicating that ORP150 overexpression in the liver reduces insulin resistance and thus ameliorates glucose tolerance in C57BL/KsJ-db/db mice. We also evaluated endogenous hepatic glucose production (HGP) in Ad-S-ORP-treated mice using tracer methods. HGP was significantly lower in Ad-S-ORP-treated mice compared with Ad-GFP-treated mice (9.5 ± 3.0 *versus* 18.0 ± 4.5 mg/kg/min, $p < 0.05$) (Fig. 2*D*). These results indicate that the reduction of insulin resistance and amelioration of glucose tolerance by Ad-S-ORP overexpression are mainly because of the suppression of HGP.

Antisense ORP150 Overexpression in the Liver Decreases Insulin Sensitivity in Non-diabetic C57BL6 Mice—Next, to examine the effects of antisense ORP150 expression in the liver on insulin sensitivity and glucose tolerance in non-diabetic animals, we prepared an antisense ORP150-expressing adenovirus (2×10^9 pfu/ml) and a control adenovirus (Ad-GFP) and delivered each adenovirus to 8-week-old C57BL6 mice from the cervical vein. By Western blot analysis we confirmed a decrease in ORP150 expression in the liver upon adenovirus injection (Fig. 1*B*). In addition, expression levels of KDEL in Ad-AS-ORP-treated mice were higher than those in Ad-GFP-treated C57BL6 mice, although there was no difference in Bip expression levels (Fig. 1*B*). There was no difference in body weight and food intake between the two groups (data not shown). In addition, although there was no difference in nonfasting blood glucose levels (Fig. 3*A*) and in fasting blood glucose and serum insulin levels between Ad-AS-ORP-treated and Ad-GFP-treated mice (Fig. 3*B*), the intraperitoneal glucose tolerance test revealed that glucose tolerance is markedly worsened upon antisense ORP150 expression (Fig. 3*C*). Furthermore, in the euglycemic hyperinsulinemic clamp study, the GIR of Ad-AS-ORP-treated C57BL6 mice were significantly lower compared with Ad-GFP-treated mice (34.3 ± 3.5 *versus* 64.4 ± 6.3 mg/kg/min, $p < 0.05$) (Fig. 3*D*), indicating that ER stress in the liver reduces insulin sensitivity in C57BL6 mice. Furthermore, we evaluated HGP in Ad-AS-ORP-treated mice using tracer methods. HGP in Ad-AS-ORP-treated mice was significantly greater than in Ad-GFP-treated mice (18.6 ± 2.1 *versus* 5.8 ± 2.0 mg/kg/min, $p < 0.05$) (Fig. 3*D*). These results indicate that antisense ORP150 expression decreases insulin sensitivity at least in part by increasing HGP in non-diabetic mice.

ER Stress in the Liver Is Associated with the Phosphorylation Status of Insulin Signaling Molecules—To examine the molecular mechanisms involved in the alteration of insulin action by ER stress in our experiments, we evaluated the phosphorylation state of IRS-1 and Akt in the liver, which are key molecules

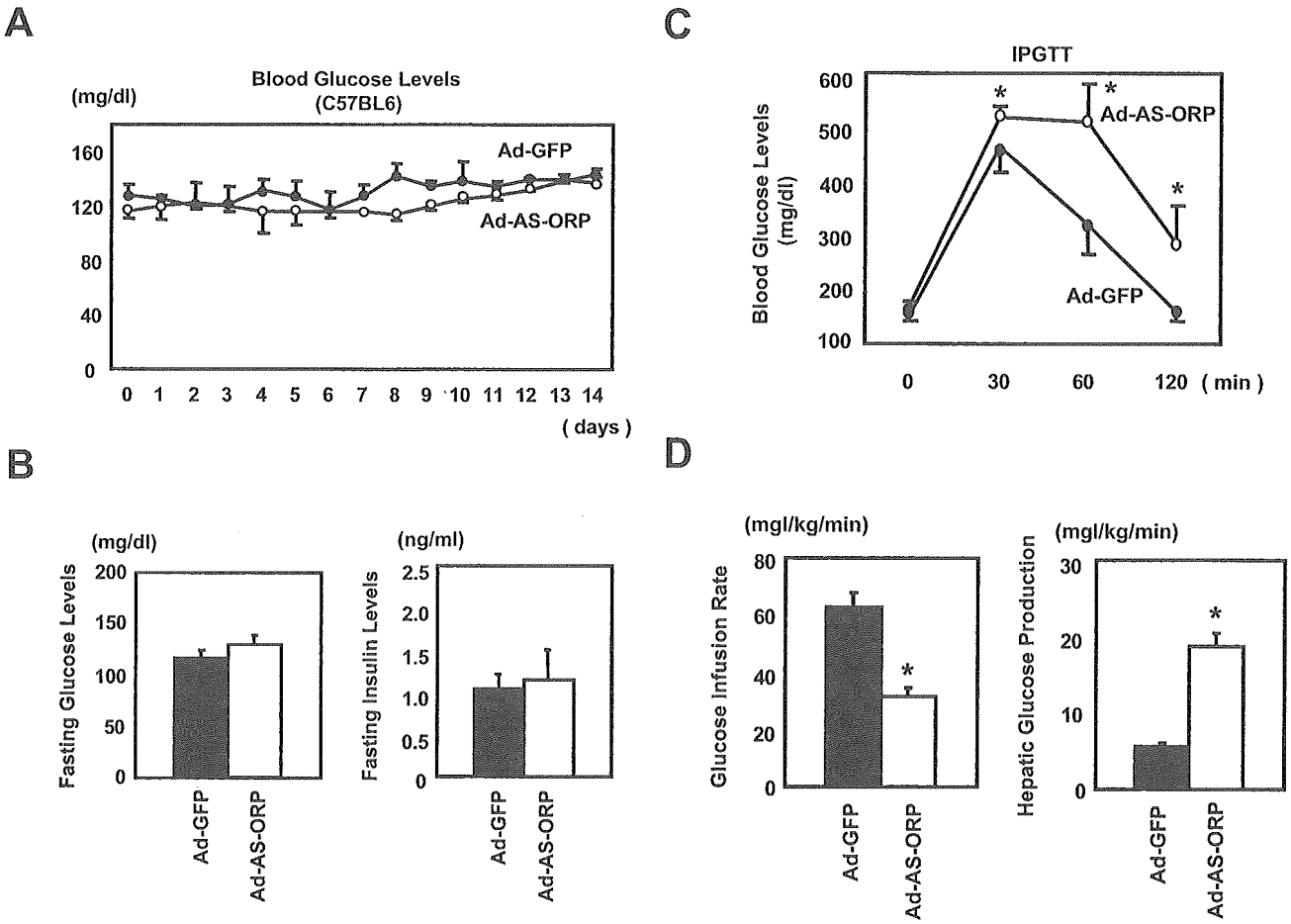

FIG. 3. **Effects of adenoviral antisense ORP overexpression in the liver on insulin resistance and glucose tolerance in C57BL6 mice.** *A*, nonfasting blood glucose levels in C57BL6 mice treated with Ad-AS-ORP or Ad-GFP ($n = 6$). *B*, fasting blood glucose and serum insulin levels in C57BL6 mice 2 weeks after injection with Ad-AS-ORP or Ad-GFP ($n = 6$). *C*, glucose tolerance in C57BL6 mice treated with Ad-AS-ORP or Ad-GFP. Two weeks after the adenovirus injection, intraperitoneal glucose tolerance tests (*IPGTT*) were performed. After a 6-h fast, glucose was injected intraperitoneally at a dose of 2.0 g/kg body weight, and blood glucose levels were measured (*, $p < 0.05$, $n = 6$). *D*, glucose infusion rate and endogeous hepatic glucose production in C57BL6 mice treated with Ad-AS-ORP or Ad-GFP. Two weeks after the adenovirus injection, glucose infusion rate and hepatic glucose production were estimated by a euglycemic hyperinsulinemic clamp test (*, $p < 0.05$, $n = 6$).

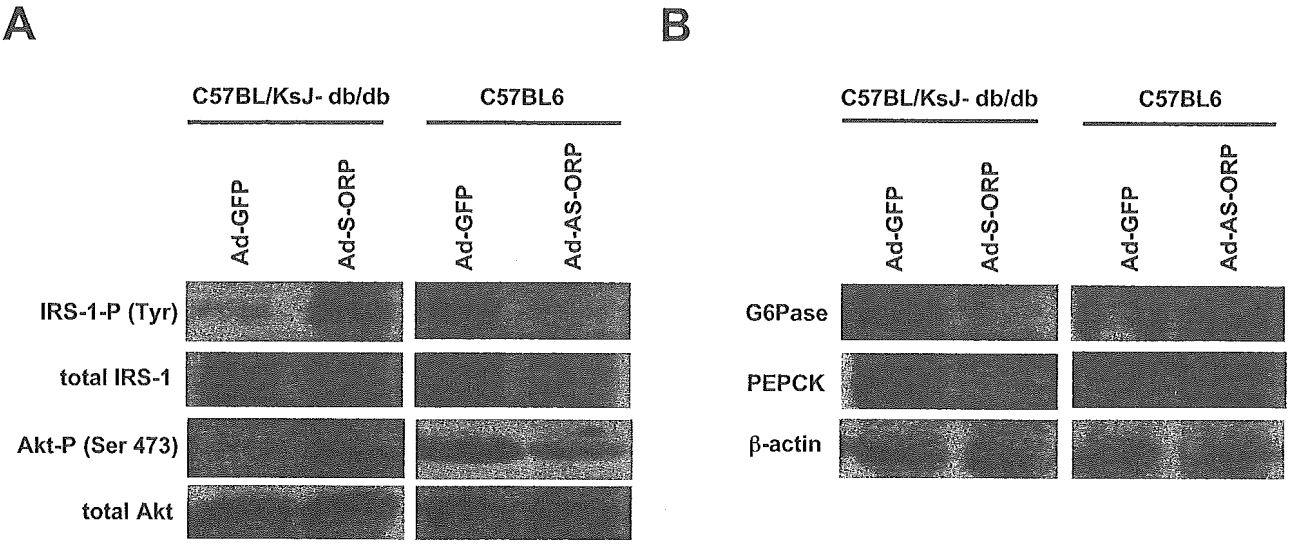

FIG. 4. **Effects of sense and antisense ORP overexpression on insulin signaling and gluconeogenesis in the liver.** *A*, effects of ER stress on insulin signaling. C57BL/KsJ-db/db mice were treated with Ad-S-ORP or Ad-GFP, and C57BL6 mice were treated with Ad-AS-ORP or Ad-GFP. Two weeks after the adenovirus injection, the expression of total and tyrosine-phophorylated forms of IRS-1 and total and phophorylated forms (Ser-473) of Akt were examined by Western blot analysis. Similar results were obtained in three independent experiments. *B*, effects of ER stress on gluconeogenesis. C57BL/KsJ-db/db mice were treated with Ad-S-ORP or Ad-GFP, and C57BL6 mice were treated with Ad-AS-ORP or Ad-GFP. Two weeks after the adenovirus injection, mRNA levels of phosphoenolpyruvate carboxykinase and glucose-6-phosphatase, key enzymes of gluconeogenesis, were examined by Northern blot analysis. Similar results were obtained in three independent experiments.

for insulin signaling. IRS-1 tyrosine phosphorylation was markedly increased in Ad-S-ORP-treated C57BL/KsJ-db/db mice compared with Ad-GFP-treated mice (Fig. 4*A*). Concomitantly, an increase in Akt serine 473 phosphorylation was observed in Ad-S-ORP-treated C57BL/KsJ-db/db mice compared with Ad-GFP-treated mice (Fig. 4*A*). In contrast, IRS-1 tyrosine phosphorylation was decreased in Ad-AS-ORP-treated mice compared with Ad-GFP-treated mice (Fig. 4*A*). A decrease in Akt serine 473 phosphorylation was observed in Ad-AS-ORP-treated C57BL6 mice compared with Ad-GFP-treated mice (Fig. 4*A*). We next examined the expression levels of the key gluconeogenic enzymes phosphoenolpyruvate carboxykinase (PEPCK) and glucose-6-phosphatase (G6Pase), both of which are known to be regulated by insulin signaling. The expression of both PEPCK and G6Pase was markedly decreased by Ad-S-ORP treatment in C57BL/KsJ-db/db mice (Fig. 4*B*). In contrast, expression of both enzymes was increased upon treatment with Ad-AS-ORP in C57BL6 mice (Fig. 4*B*). These results indicate that reduction of ER stress enhances insulin signaling, which leads to a decrease in gluconeogenesis and amelioration of glucose tolerance.

In conclusion, sense ORP150 overexpression decreased insulin resistance and markedly improved glycemic control in diabetic model animals; in contrast, antisense ORP150 expression induced insulin resistance in non-diabetic control mice, indicating that ER stress plays a crucial role in the insulin resistance found in diabetes. ER stress could thus be a potential therapeutic target for diabetes.

Acknowledgments—We thank Yuko Sasaki for excellent technical assistance and Chikayo Yokogawa for efficient secretarial assistance. We also thank Dr. Helena Akiko Popiel for valuable comments on the manuscript.

REFERENCES

1. Saltiel, A. R., and Kahn, C. R. (2001) *Nature* **414,** 799–806
2. Shulman, G. I. (2000) *J. Clin. Investig.* **106,** 171–176
3. Weir, G. C., Laybutt, D. R., Kaneto, H., Bonner-Weir, S., and Sharma, A. (2001) *Diabetes* **50,** Suppl. 1, 154–159
4. Robertson, R. P., Harmon, J., Tran, P. O., and Poitout, V. (2004) *Diabetes* **53,** Suppl. 1, 119–124
5. Wang, X.-Z., Harding, H. P., Zhang, Y., Jolicoeur, E. M., Kuroda, M., and Ron, D (1998) *EMBO J.* **17,** 5708–5717
6. Tirasophon, W., Welihinda, A. A., and Kaufman, R. J. (1998) *Genes Dev.* **12,** 1812–1824
7. Harding, H. P., Zhang, Y., and Ron, D. (1999) *Nature* **397,** 271–274
8. Aridor, M., and Balch, W. E. (1999) *Nat. Med.* **5,** 745–751
9. Don, D. (2002) *J. Clin. Investig.* **110,** 1383–1388
10. Inoue, H., Tanizawa, Y., Wasson, J., Behn, P., Kalidas, K., Bernal-Mizrachi, E., Mueckler, M., Marshall, H., Donis-Keller, H., Crock, P., Rogers, D., Mikuni, M., Kumashiro, H., Higashi, K., Sobue, G., Oka, Y., and Permutt, M. A. (1998) *Nat. Genet.* **20,** 143–148
11. Harding, H. P., Zeng, H., Zhang, Y., Jungries, R., Chung, P., Plesken, H., Sabatini, D. D., and Ron, D. (2001) *Mol. Cell* **7,** 1153–1163
12. Harding, H. P., and Ron, D. (2002) *Diabetes* **51,** Suppl. 3, 455-461
13. Oyadomari, S., Takeda, K., Takiguchi, M., Gotoh, T., Matsumoto, M., Wada, I., Akira, S., Araki, E., and Mori, M. (2001) *Proc. Natl. Acad. Sci. U. S. A.* **98,** 10845–10850
14. Oyadomari, S., Koizumi, A., Takeda, K., Gotoh, T., Akira, S., Araki, E., and Mori, M. (2002) *J. Clin. Investig.* **109,** 525–532
15. Kuwabara, K., Matsumoto, M., Ikeda, J., Hori, O., Ogawa, S., Maeda, Y., Kitagawa, K., Imuta, N., Kinoshita, T., Stern, D. M., Yanagi, H., and Kamada, T. (1996) *J. Biol. Chem.* **271,** 5025–5032
16. Tamatani, M., Matsuyama, T., Yamaguchi, A., Mitsuda, N., Tsukamoto, Y., Taniguchi, M., Che, Y. H., Ozawa, K., Hori, O., Nishimura, H., Yamashita, A., Okabe, M., Yanagi, H., Stern, D. M., Ogawa, S., and Tohyama, M. (2001) *Nat. Med.* **7,** 317–323

ELSEVIER

Atherosclerosis 183 (2005) 369–371

ATHEROSCLEROSIS

www.elsevier.com/locate/atherosclerosis

Letter to the Editor

Lipid-lowering with atorvastatin improves tissue characteristics of carotid plaque

Dear Editors,

Statins can attenuate the increase of atheroma volume and reduce coronary events [1,2]. However, whether statins affect the tissue characteristics of the carotid artery remains to be fully evaluated. Integrated backscatter (IBS) signal obtained by ultrasound examination of the carotid artery reflects the acoustic characteristics of the carotid wall and can differentiate among the tissue characteristics of arterial plaque [3,4]. This is a preliminary study to assess the effects of atorvastatin on carotid atherosclerosis using intima-media thickness (IMT) and IBS analyses.

Subjects were selected from outpatients at Osaka Police Hospital. Those who were suffering from severe renal or hepatic disease, apparent cardiovascular disease or malignancy were excluded. A total of 20 patients with hyperlipidemia (total cholesterol (T-chol) concentrations above 220 mg/dl or low density lipoprotein cholesterol (LDL-C) concentrations above 140 mg/dl) but who had not been previously treated with lipid-lowering agent were recruited and randomized to an atorvastatin-treatment group (5–20 mg/day, $n=10$) or a non-statin-treatment group ($n=10$) treated with bezafibrate (400 mg/day) or probucol (500 mg/day). As a control, ten subjects without hyperlipidemia were randomly recruited from outpatients. None of these patients received other hypolipidemic drugs or anti-platelet drugs. The other drugs administered remained the same during the observation period.

Ultrasonographic scanning of the carotid artery was performed with the SONOS 5500 (Philips Medical Systems) using an electrical linear transducer (midfrequency of 7.5 MHz) at the beginning and the end of the observation period of 12 months. Initially, conventional B-mode imaging of the extracranial common carotid artery, the carotid bulb, and the internal carotid artery was performed. The site of the greatest IMT including the plaque lesion was defined as maxIMT. IBS analysis was performed with a software package "Acoustic Densitometry" with the SONOS 5500. In this system, IBS is calculated as the average power of the ultrasonic backscattered signal from the region of interest (ROI) and represents the tissue characteristics [4]. IBS data in the intima-media complex and those in the adventitia were sampled at a location close to where the maxIMT was measured. Next, the IBS values in the intima-media complex were corrected by subtracting the IBS values in the adventitia as follows:

corrected-IBS = IBS values in intima-media complex

−IBS values in the adventitia

The productions of maxIMT and corrected-IBS (IMT–IBS product) were also calculated.

Clinical, biochemical and acoustic parameters before and after the follow-up period are expressed in Table 1. At baseline, T-chol and LDL-C were significantly higher in non-statin-treatment group and atorvastatin-treatment group than in the control group. As compared with the control group, atorvastatin-treatment group showed significantly higher maxIMT and lower corrected-IBS and IMT–IBS product. As a group ($n=30$), the corrected-IBS inversely correlated with T-chol ($r=0.544$, $p=0.0015$), LDL-C ($r=0.552$, $p=0.0012$), and TG ($r=0.490$, $p=0.0053$) and positively correlated with HDL-C ($r=0.368$, $p=0.045$). High LDL-C ($F=10.6$) and high TG ($F=7.4$) were demonstrated to be the only independent risk factors for low IBS value in stepwise multivariate regression analysis. The other clinical parameters did not significantly correlate with the IBS value. These data suggest that hyperlipidemia is closely associated with the acoustic characteristics of the carotid wall.

During the treatment period of 12.8 months, mean serum T-chol levels significantly decreased in atorvastatin-treatment group and non-statin-treatment group. While serum LDL-C levels significantly decreased in the atorvastatin-treatment group, the reduction was not significant in the non-statin-treatment group (Table 1).

The mean values of maxIMT at the beginning and end of the observation period were not significantly different in any group. In the atorvastatin-treatment group, however, the relative change in maxIMT showed a regressive tendency compared with a progressive tendency in the control group. After the treatment period, the corrected-IBS and IMT–IBS product values significantly increased in the atorvastatin-treatment group (from -21.7 ± 3.6 to -17.6 ± 3.1 dB, $p<0.01$ and from -39.5 ± 15.0 to -31.9 ± 15.5 mm × dB, $p=0.0027$, respectively). However, no significant difference was seen in the control group and the non-statin-treatment group (Table 1). The significant increase of the corrected-IBS

0021-9150/$ – see front matter
doi:10.1016/j.atherosclerosis.2005.08.011

Table 1
clinical and biochemical parameters before and after the follow-up period

	Control ($n=10$)		Non-statin-treatment ($n=10$)		Atorvastatin-group ($n=10$)	
	Before	After	Before	After	Before	After
Gender (male/female)	6/4		5/5		6/4	
Age (years)	59.7 ± 10.3		57.4 ± 9.6		63.8 ± 8.1	
BMI (kg/mm^2)	23.2 ± 3.8	23.1 ± 3.8	22.6 ± 2.4	24.2 ± 2.4	23.6 ± 1.5	23.7 ± 1.7
FPG (mmol/l)	6.40 ± 1.22	6.27 ± 2.39	6.28 ± 1.33	6.60 ± 2.33	6.24 ± 1.04	6.60 ± 1.72
T-chol (mmol/l)	4.94 ± 0.44	4.82 ± 0.46	6.04 ± 0.48[a]	5.62 ± 0.73*	6.22 ± 0.47[a]	4.75 ± 0.57*
LDL-C (mmol/l)	2.94 ± 0.40	2.96 ± 0.60	3.92 ± 0.29[a]	3.65 ± 0.62	3.95 ± 0.31[a]	2.61 ± 0.41*
HDL-C (mmol/l)	1.48 ± 0.34	1.28 ± 0.37*	1.37 ± 0.41	1.27 ± 0.33	1.55 ± 0.20	1.47 ± 0.21
TG (mmol/l)	1.20 ± 0.55	1.02 ± 0.41	1.52 ± 0.63	1.47 ± 0.62	1.43 ± 0.68	1.32 ± 0.38
sBP (mmHg)	135 ± 10	134 ± 15	139 ± 6	132 ± 9	130 ± 8[b]	125 ± 11
dBP (mmHg)	76 ± 7	76 ± 9	81 ± 7	72 ± 9	77 ± 10	74 ± 9
Smoking (yes/no)	1/9	1/9	3/7	3/7	2/8	2/8
maxIMT (mm)	1.29 ± 0.17	1.41 ± 0.29	1.68 ± 0.55	1.67 ± 0.60	1.84 ± 0.67[a]	1.78 ± 0.77
Corrected-IBS (dB)	−17.6 ± 5.0	−18.5 ± 3.6	−20.8 ± 2.6	−21.2 ± 2.6	−21.7 ± 3.6[a]	−17.6 ± 3.1*
IMT–IBS product	−22.6 ± 6.2	−26.1 ± 6.8	−34.1 ± 8.4	−34.8 ± 10.9	−39.5 ± 15.0[a]	−31.9 ± 15.5*

Data are shown as mean ± S.D. Differences among the three groups were determined by one-way analysis of variance (ANOVA). Paired t-tests were used to compare the biochemical and acoustic parameters before and after 1 year in each of the defined group of patients. BMI, body mass index; FPG, fasting plasma glucose; HbA1C, hemoglobin A1C; T-chol, total cholesterol; LDL-C, LDL-cholesterol; HDL-C, HDL cholesterol; TG, triglyceride; sBP, systolic blood pressure; dBP, diastolic blood pressure; maxIMT, maximum IMT; IMT–IBS product; corrected-IBS × maximum IMT.

[a] Significant difference vs. control.

[b] Significant difference vs. non-statin-treatment group.

* $p<0.05$ vs. values before treatment.

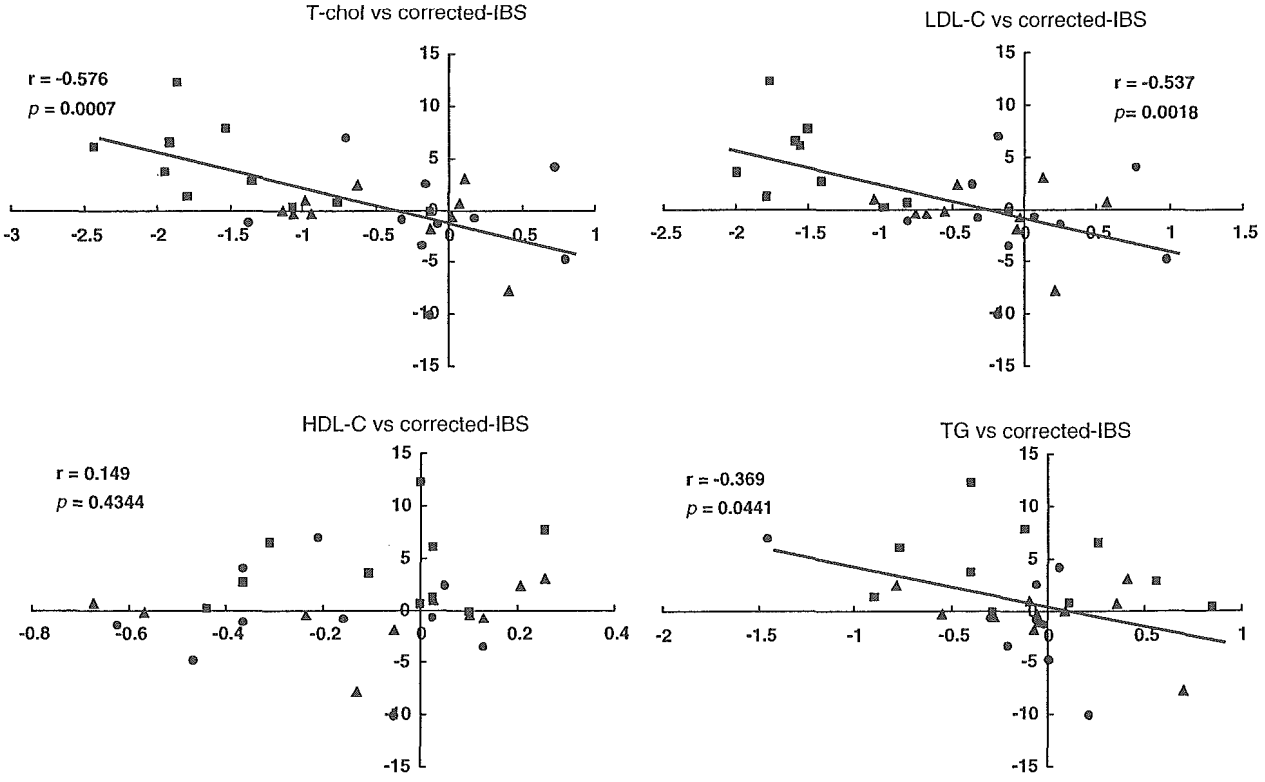

Fig. 1. Correlation between the improvement in lipid parameters and the changes in acoustic parameters. Close circles; control group, close triangles; non-statin-treatment group, close squares; atorvastatin-treatment group. As a group ($n=30$), changes in corrected-IBS value inversely correlated with changes in T-chol ($r=-0.576$, $p=0.0007$), LDL-C ($r=-0.537$, $p=0.0018$) and TG ($r=-0.369$, $p=0.0441$) but did not correlate with HDL-C.

in the atorvastatin-treatment group may reflect the improvement of tissue characteristics of carotid artery, since previous studies showed that a low-IBS-value represents lipid-rich tissue [3,4]. Similarly, the significant increase of the IMT–IBS product in the atorvastatin-treatment group may be associated with the stabilization of the atheromatous lesion in the carotid, since IMT–IBS product, which seems to reflect both the size and quality of a plaque lesion, is reported to be associated with recent history of acute coronary syndrome and atherothrombotic brain infarction [5]. Interestingly, as a group ($n=30$), changes in corrected-IBS inversely correlated with changes in T-chol ($r=-0.576$, $p=0.0007$), LDL-C ($r=-0.537$, $p=0.0018$) and TG ($r=-0.369$, $p=0.0441$) (Fig. 1). The stepwise multivariate regression analysis revealed the increase of LDL-C ($F=11.4$) to be the only independent risk factor for the decrease of corrected-IBS. Changes in IMT–IBS product also correlated inversely with changes in T-chol ($r=-0.583$, $p=0.0005$) and LDL-C ($r=-0.538$, $p=0.0018$). Since the increase of corrected-IBS and IMT–IBS product were strongly correlated with the reduction of LDL-C, the beneficial effect brought on by the atorvastatin-treatment appeared to be mainly related to the degree of lipid-lowering itself. However, the pleiotropic effects of atorvastatin independent of lipid reduction remain to be examined in further studies.

In conclusion, the results of the acoustic analysis of the carotid arterial wall suggest that atorvastatin has beneficial effects on tissue characteristics of the carotid artery.

References

[1] Sacks FM, Pfeffer MA, Moye LA, et al. The effect of pravastatin on coronary events after myocardial infarction in patients with average cholesterol levels. N Engl J Med 1996;335:1001–9.

[2] Nissen SE, Tuzcu EM, Schoenhagen P, et al., REVERSAL Investigators. Effect of intensive compared with moderate lipid-lowering therapy on progression of coronary atherosclerosis. JAMA 2004;291:1071–80.

[3] Urbani MP, Picano E, Parenti G, et al. In vivo radiofrequency-based ultrasonic tissue characterization of the atherosclerotic plaque. Stroke 1993;24:1507–12.

[4] Kawasaki M, Takatsu H, Noda T, et al. Noninvasive quantitative tissue characterization and two-dimensional color-coded map of human atherosclerotic lesions using ultrasound integrated backscatter: comparison between histology and integrated backscatter images. J Am Coll Cardiol 2001;38:486–92.

[5] Katakami N, Yamasaki Y, Kosugi K, et al. Tissue characterization identifies subjects with high risk of cardiovascular diseases. Diab Res Clin Pract 2004;63:93–102.

Naoto Katakami*
Ken'ya Sakamoto
Hideaki Kaneto
Munehide Matsuhisa
Masatsugu Hori
Yoshimitsu Yamasaki
Department of Internal Medicine and Therapeutics, Osaka University Graduate School of Medicine, 2-2, Yamadaoka, Suita, Osaka 565-0871, Japan

Keisuke Kosugi
Hidehiko Waki
Osaka Police Hospital, Osaka, Japan

* Corresponding author. Tel.: +81 6 6879 3633; fax: +81 6 6879 3639.
E-mail address: katakami@medone.med.osaka-u.ac.jp (N. Katakami)

12 July 2005
Available online 12 September 2005

Decreased Endogenous Secretory Advanced Glycation End Product Receptor in Type 1 Diabetic Patients

Its possible association with diabetic vascular complications

NAOTO KATAKAMI, MD, PHD[1]
MUNEHIDE MATSUHISA, MD, PHD[1]
HIDEAKI KANETO, MD, PHD[1]
TAKA-AKI MATSUOKA, MD, PHD[1]
KEN'YA SAKAMOTO, MD, PHD[1]
YOSHIHISA NAKATANI, MD, PHD[1]
KENTARO OHTOSHI, MD, PHD[2]
RIEKO HAYAISHI-OKANO, MD, PHD[1]
KEISUKE KOSUGI, MD, PHD[2]
MASATSUGU HORI, MD, PHD[1]
YOSHIMITSU YAMASAKI, MD, PHD[1]

OBJECTIVE — The binding of advanced glycation end products (AGEs) to their receptor (RAGE) plays an important role in the development of diabetic vascular complications. In the present study, we examined circulating endogenous secretory RAGE (esRAGE) levels in subjects with type 1 diabetes and explored the possible association between esRAGE levels and the severity of diabetic vascular complications.

RESEARCH DESIGN AND METHODS — Circulating esRAGE levels in serum were examined in 67 Japanese type 1 diabetic patients (22 men and 45 women, age 24.0 ± 4.4 years [means ± SD]) and 23 age-matched healthy nondiabetic subjects (10 men and 13 women aged 24.9 ± 1.4 years). Daily urinary albumin excretion, the presence of retinopathy, and intima-media thickness (IMT) of the carotid artery were also evaluated. We further explored the association between esRAGE levels and severity of diabetic vascular complications.

RESULTS — Circulating esRAGE levels were significantly lower in subjects with type 1 diabetes than in nondiabetic subjects (0.266 ± 0.089 vs. 0.436 ± 0.121 ng/ml, respectively, $P < 0.0001$) and was inversely correlated with HbA_{1c} (A1C) levels ($r = -0.614$, $P < 0.0001$). In addition, multivariate regression analysis demonstrated that A1C was an independent risk factor for a low esRAGE value. Furthermore, circulating esRAGE levels were inversely correlated with carotid IMT ($r = -0.325$, $P = 0.0017$) and was one of the independent risk factors for IMT thickening. Furthermore, there was a significant difference ($P = 0.0124$) in esRAGE levels between patients without retinopathy (0.286 ± 0.092 ng/ml) and those with retinopathy (0.230 ± 0.074 ng/ml).

CONCLUSIONS — Circulating esRAGE levels were significantly lower in type 1 diabetic patients than in nondiabetic subjects and were inversely associated with the severity of some diabetic vascular complications.

Diabetes Care 28:2716–2721, 2005

Microvascular complications and atherosclerosis, which are accelerated in patients with prolonged duration of type 1 diabetes, lead to the impairment of quality of life and are major causes of mortality. Reducing sugars such as glucose can react nonenzymatically with the amino groups of proteins. After further complex reactions, irreversibly cross-linked, heterogeneous derivatives termed advanced glycation end products (AGEs) are formed. AGEs accumulate in circulating blood and various tissues and are implicated in the development of diabetic vascular complications (1,2). Recent studies have shown that the system of AGEs and their receptor (RAGE) plays an important role in the development of diabetic vascular complications (3–6). The binding of AGE to RAGE is known to cause phenotypic changes in various cells such as endothelial cells, smooth muscle cells, pericytes, and renal mesangial cells, leading to the pathogenesis of diabetic retinopathy, nephropathy, and macroangiopathies (7–14).

RAGE belongs to the immunoglobulin superfamily of cell surface molecules and is composed of an extracellular region containing one V-type and two C-type immunoglobulin domains (15). Human vascular cells mainly express three major RAGE mRNA variants. They encode the full-length RAGE (full-length type), a variant protein lacking the NH_2-terminal region (N-truncated type), and another variant lacking the COOH-terminal region (C-truncated type) (4,16). The mRNA for the C-truncated type contains the 5′ part of intron 9 and encodes a receptor protein consisting of 347 amino acids with a 22-amino acid signal sequence and a unique 16-amino acid stretch. The C-truncated type lacks the transmembrane domain and is secreted extracellularly and detected in human sera as endogenous secretory (es) RAGE. Interestingly, it was reported that esRAGE binds to an AGE ligand and has an activity that neutralizes AGE actions (11,14,16, 17). Thus, it is possible that human circulating esRAGE potentially influences the development of diabetic vascular complications. Indeed, various studies have demonstrated that addition or overexpression of the C-truncated RAGE attenuates the progression of diabetic vascular complications (13,18). However, very little informa-

From the [1]Department of Internal Medicine and Therapeutics (A8), Osaka University Graduate School of Medicine, Osaka, Japan; and the [2]Department of Internal Medicine, Osaka Police Hospital, Osaka, Japan.

Address correspondence and reprint requests to Naoto Katakami, MD, PhD, Department of Internal Medicine and Therapeutics (A8), Osaka University Graduate School of Medicine, 2-2, Yamadaoka, Suita, Osaka 565-0871, Japan. E-mail: katakami@medone.med.osaka-u.ac.jp.

Received for publication 17 May 2005 and accepted in revised form 28 July 2005.

Abbreviations: AGE, advanced glycation end product; DBP, diastolic blood pressure; es, endogenous secretory; hs-CRP, high-sensitivity C-reactive protein; IMT, intima-media thickness; RAGE, receptor for AGEs; SBP, systolic blood pressure.

A table elsewhere in this issue shows conventional and Système International (SI) units and conversion factors for many substances.

Table 1—*Baseline characteristics of the study subjects*

	Control subjects	Type 1 diabetic subjects	*P*
n	23	67	—
Sex (male/female)	10/13	22/45	NS*
Age (years)	24.9 ± 1.4	24.0 ± 4.4	NS
Duration of diabetes (years)	—	14.5 ± 6.2	—
Smoking (yes/no)	3/20	9/58	NS*
BMI (kg/m^2)	20.4 ± 2.0	22.2 ± 2.5	0.0048
SBP (mmHg)	113 ± 12	117 ± 13	NS
DBP (mmHg)	66 ± 8	73 ± 9	0.0049
A1C (%)	4.64 ± 0.31	7.85 ± 1.35	<0.0001
Total cholesterol (mmol/l)	4.69 ± 0.75	4.84 ± 0.75	NS
HDL cholesterol (mmol/l)	1.71 ± 0.34	1.86 ± 0.37	NS
Triglycerides (mmol/l)	0.76 ± 0.27	1.10 ± 0.72	0.0353
esRAGE (ng/ml)	0.436 ± 0.121	0.266 ± 0.089	<0.0001
hs-CRP (mg/l)	0.376 ± 0.744 (0.05–3.4)	1.064 ± 1.929 (0.05–11.9)	0.0011†
Urinary albumin excretion (mg/day)	—	17.5 ± 46.6	—
Retinopathy (NDR/BDR/PDR)	—	43/20/4	—
IMT (mm)	0.58 ± 0.06	0.63 ± 0.11	0.0396

Data are means ± SD or means ± SD (range) unless otherwise indicated. Student's *t* test was performed as indicated. *χ^2 test, †Mann-Whitney *U* test. BDR, background diabetic retinopathy; NDR, no diabetic retinopathy; PDR, proliferative diabetic retinopathy.

tion has been obtained about circulating esRAGE levels in human subjects.

In the present study, we examined circulating esRAGE levels in type 1 diabetic patients. We also explored the possible association between esRAGE levels and the severity of diabetic vascular complications.

RESEARCH DESIGN AND METHODS— A total of 67 Japanese type 1 diabetic patients (22 men and 45 women, age 24.0 ± 4.4 years [means ± SD] with duration of diabetes of 14.5 ± 6.2 years and daily urine C-peptide concentration of 5.6 ± 9.2 μg/day) undergoing periodic follow-up examinations at the Diabetes Clinic of Osaka University Hospital and the Osaka Police Hospital were enrolled in this study. The diagnoses of type 1 diabetes were done by diabetologists. All patients were treated with insulin alone and performed at least three or four daily insulin injections. The daily insulin dose was 0.86 ± 0.25 units/kg. As control subjects, we also enrolled 23 age-matched healthy nondiabetic individuals (10 men and 13 women, age 24.9 ± 1.4 years). None of the subjects had any clinical evidence of infection, connective tissue disease, liver dysfunction, or angiopathy. None of the subjects was taking any oral hypoglycemic drugs or antihypertensive, antiplatelet, or lipid-lowering medications at the time of the study. After a full explanation of the study, written informed consent was obtained from each subject. The study was approved by the Ethical Committee for Human Studies at Osaka University Graduate School of Medicine.

Fasting blood samples were collected, and the laboratory analyses were performed by SRL (Tokyo, Japan) as follows. Serum total cholesterol and HDL cholesterol, serum triglyceride, and HbA_{1c} (A1C) levels were measured using standard laboratory protocols. High-sensitivity C-reactive protein (hs-CRP) concentration was measured by enzyme-linked immunosorbent assay. The intra-assay coefficient of variation for repeated hs-CRP measurements ranged from 0.80 to 1.72%.

Subjects with diabetes submitted urine samples that had been collected at home over the previous 24 h. Written instructions and a careful explanation regarding the procedure for urine collection were given to each subject. Most of the patients were familiar with the method for collecting urine at home. Nevertheless, a urine sample was discarded when there was any doubt about its collection. The 24-h urine samples collected from each subject were used to determine urinary albumin excretion. According to the amount of their daily urinary albumin excretion, patients were classified into the normoalbuminuria group (urinary albumin excretion <30 mg/day), microalbuminuria group (urinary albumin excretion 30–300 mg/day), and macroalbuminuria group (urinary albumin excretion >300 mg/day). The presence of retinopathy was diagnosed by ophthalmologists based on the findings of funduscopy. Smokers were classified as having a current smoking habit.

Measurement of circulating esRAGE

To measure the concentration of human circulating esRAGE in serum, we used the B-Bridge esRAGE ELISA Kit (manufactured by Daiichi Fine Chemicals, Takaoka, Japan, and distributed by B-Bridge International). Measurements were performed following the manufacturer's instructions. The intra-assay coefficient of variation for repeated esRAGE measurements ranged from 3.5 to 6.7%.

Measurement of intima-media thickness

To estimate early-stage atherosclerosis, ultrasonographic scanning of the carotid artery was performed using an echotomographic system (Toshiba, Tokyo, Japan) with an electrical liner transducer (mid-frequency 8.0 MHz). The detection limit of this echo system using 8.0 MHz was 0.1 mm. Scanning of the extracranial common carotid artery, the carotid bulb, and the internal carotid artery in the neck was performed bilaterally from three different longitudinal projections (i.e., anterior oblique, lateral, and posterior oblique) as well as the transverse projections, as reported in our previous studies (19,20). The intima-media thickness (IMT) defined by Pignoli et al. (21) was measured as follows. At each longitudinal projection, the site of the greatest thickness including a plaque lesion was sought along the arterial walls. Three determinations of

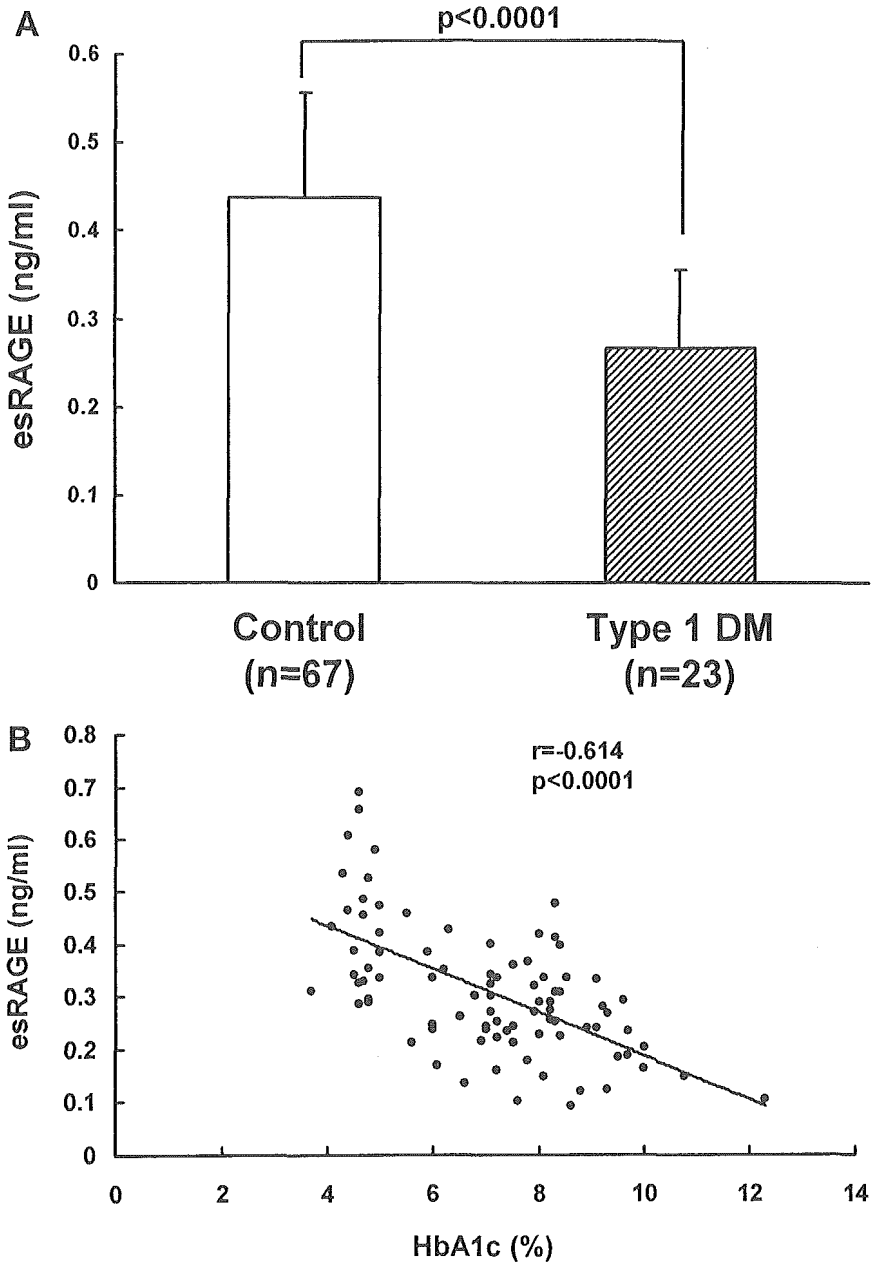

Figure 1—A: *Comparison of circulating esRAGE levels between type 1 diabetic patients and nondiabetic subjects. esRAGE levels were significantly lower in type 1 diabetic patients than in nondiabetic subjects (0.266 ± 0.089 vs. 0.436 ± 0.121 ng/ml, P < 0.0001).* B: *Association between circulating esRAGE levels and glycemic control. esRAGE levels were inversely correlated with A1C levels (r = −0.614, P < 0.0001).*

IMT were conducted at the site of the thickest point and two adjacent points (located 1 cm upstream and 1 cm downstream from the thickest point). These three determinations were averaged (mean IMT). The greatest value among the six mean IMTs (three from the left and three from right) was used as the representative value for each individual. All ultrasound scans were performed by an experienced sonographer, and an experienced physician performed the determination of IMTs on the photographs. These two individuals were unaware of the subject's study group and clinical characteristics. Reproducibility of the IMT measurement was examined 1 week later in 30 participants with type 1 diabetes by the same sonographer and the same physician. The mean difference in IMT between these two determinations was 0.04 mm, and the standard deviation was 0.07 mm, demonstrating good reproducibility for repeated measurements.

Statistical analysis

Data are given as means ± SD. Means or proportions for clinical characteristics were computed for the case and control subjects. Data between the two groups were compared by a two-tailed unpaired Student's *t* test, and data among more than two groups were compared by a one-way ANOVA followed by Scheffe's test. Differences in proportions were tested using the χ^2 test. Because the hs-CRP distribution was skewed to the left, the median concentrations were computed for these parameters, and the significance of any differences between the patient and control subjects was determined using the Mann-Whitney *U* test. Single linear univariate correlations (Pearson's correlation coefficients) and forward and backward stepwise multivariate regression analyses

Table 2—*Correlation between esRAGE and variables in all subjects*

	Univariate*		Multivariate†		
	r	*P*	β	*F*	*P*
Age (years)	−0.052	NS			
Sex (male/female)	—	NS			
Diabetes (yes/no)	—	0.0001			
Duration of diabetes (years)	−0.127	NS			
Smoking (yes/no)	—	NS			
BMI (kg/m^2)	−0.363	0.0005	−0.012	9.0	0.0035
SBP (mmHg)	−0.139	NS			
DBP (mmHg)	−0.274	0.0095			
A1C (%)	−0.614	<0.0001	−0.038	46.1	<0.00001
Total cholesterol (mmol/l)	−0.138	NS			
HDL cholesterol (mmol/l)	−0.022	NS			
Triglycerides (mmol/l)	−0.252	0.0175			
Log_{10} CRP(mg/l)	−0.314	0.0024			
R^2	—	—	0.414	—	—

*Pearson's univariate correlation coefficients. †A stepwise multivariate regression analysis was performed. Sex: male = 1, female = 0; smoking: yes = 1, no = 0. β: partial regression coefficient.

were performed to evaluate the relationship between esRAGE and the following variables: sex, age, duration of diabetes, BMI, systolic blood pressure (SBP), diastolic blood pressure (DBP), smoking habit, A1C, total cholesterol, triglycerides, HDL cholesterol, and hs-CRP (logarithmically transformed data). Single linear univariate correlations and forward and backward stepwise multivariate regression analyses were performed to evaluate the relationship between meanIMT and the following variables: sex, age, BMI, SBP, DBP, smoking habit, A1C, total cholesterol, triglycerides, HDL cholesterol, hs-CRP (logarithmically transformed data), and esRAGE. For the forward and backward stepwise multivariate regression analyses, the *F* value for the inclusion and exclusion of variables was set at 2.0. These statistical analyses were performed using Stat-View statistical software (version 5.0 for Windows; Abacus Concepts, Berkeley, CA) and HALBOU statistical software (Gendai Sugaku-sha, Kyoto, Japan) on a personal computer. The threshold of statistical significance was defined as $P < 0.05$.

RESULTS

Circulating esRAGE levels are lower in type 1 diabetic patients than in nondiabetic subjects

Clinical and biochemical characteristics of the study subjects are presented in Table 1. BMI, DBP, A1C, triglyceride levels, and hs-CRP levels were significantly higher in subjects with type 1 diabetes than in nondiabetic subjects ($P < 0.05$). There was no significant difference between the two groups regarding the other clinical parameters such as age, sex, current smoking habit, SBP, total cholesterol, and HDL cholesterol. Circulating esRAGE levels were significantly lower in subjects with type 1 diabetes than in nondiabetic subjects (0.266 ± 0.089 vs. 0.436 ± 0.121 ng/ml, $P < 0.0001$) (Fig. 1*A*). Furthermore, serum esRAGE levels were inversely correlated with A1C levels ($r = -0.614$, $P < 0.0001$) (Fig. 1*B*). Serum esRAGE levels were also inversely correlated with BMI ($r = -0.363$, $P = 0.0005$), DBP ($r = -0.274$, $P = 0.0095$), triglyceride levels ($r = -0.252$, $P = 0.0175$), and the common logarithm of hs-CRP ($r = -0.314$, $P = 0.0024$). Furthermore, we performed a stepwise multivariate regression analysis and found that BMI ($F = 9.0$, $P = 0.0035$) and A1C ($F = 46.1$, $P < 0.00001$) were independent risk factors for a low esRAGE value (Table 2).

Circulating esRAGE levels are inversely correlated with the severity of macroangiopathy

Mean IMT was significantly greater in patients with type 1 diabetes than in nondiabetic subjects (0.63 ± 0.11 mm vs. 0.58 ± 0.06 mm, respectively, $P = 0.0396$). Furthermore, circulating esRAGE levels were inversely correlated with mean IMT ($r = -0.325$, $P = 0.0017$) (Fig. 2*B*). When only the diabetic subjects were analyzed, the correlations between esRAGE and IMT or A1C were weakened. However, there were still statistically significant correlations between esRAGE and IMT ($r = -0.289$, $P = 0.0171$) or A1C levels ($r = -0.370$, $P = 0.019$). Positive correlations were also observed between mean IMT and sex ($r = 0.271$, $P = 0.0098$), BMI ($r = 0.256$, $P = 0.0165$), and DBP ($r = 0.284$, $P = 0.0070$). To demonstrate that esRAGE is a determinant of mean IMT independent of conventional risk factors, we performed a stepwise multivariate regression analysis and found that esRAGE ($F = 4.6$, $P = 0.035$) and sex ($F = 4.1$, $P = 0.047$) were variables that interacted independently of mean IMT in all subjects. Taken together, these results show that the esRAGE level inversely correlates with the severity of macroangiopathy.

Circulating esRAGE levels tend to be inversely correlated with the severity of microangiopathy

Circulating esRAGE levels in patients without retinopathy ($n = 43$), with background retinopathy ($n = 20$), and with proliferative retinopathy (PDR) ($n = 4$) were 0.286 ± 0.092, 0.244 ± 0.068, and 0.162 ± 0.067 ng/ml, respectively. There was a significant difference ($P = 0.0124$) in circulating esRAGE levels between subjects without retinopathy (0.286 ± 0.092 ng/ml) and with retinopathy (background retinopathy + proliferative retinopathy groups, 0.230 ± 0.074 ng/ml) (Fig. 2*A*). Although the duration of diabetes was significantly longer in the subjects with retinopathy than in those without it (17.3 ± 4.0 vs. 12.9 ± 6.7 years, $P = 0.0049$), there was no significant difference among the groups in all other parameters.

On the other hand, there was no significant difference in circulating esRAGE levels between patients with microalbuminuria ($n = 9$, 0.287 ± 0.086 ng/ml) and without it ($n = 53$, 0.266 ± 0.087 ng/ml). Also, there was no significant difference in all other parameters between the groups. Although there was a weak inverse correlation between circulating esRAGE levels and daily urinary albumin excretion, it did not reach statistical significance ($r = -0.242$, $P = 0.060$).

CONCLUSIONS— In this study, we found that circulating esRAGE levels were significantly lower in young subjects with type 1 diabetes than in nondiabetic subjects (0.266 ± 0.089 vs. 0.436 ± 0.121 ng/ml, $P < 0.0001$) (Fig. 1). Furthermore, univariate regression analysis showed a strong inverse correlation be-

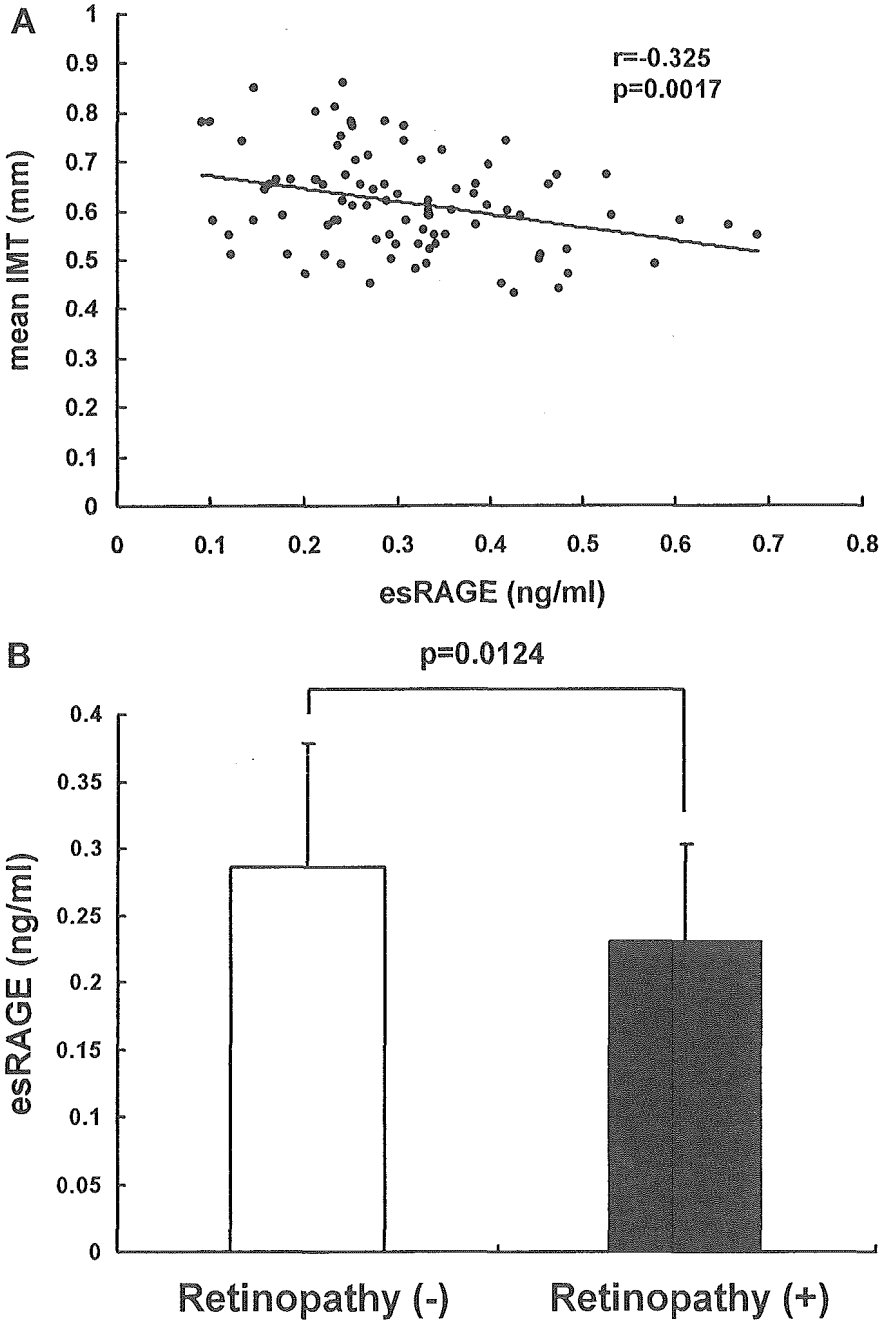

Figure 2—A: *Association between circulating esRAGE level and severity of diabetic macroangiopathy. esRAGE levels were inversely correlated with mean IMT* (r = −0.325, P = 0.0017). B: *Association between circulating esRAGE levels and severity of diabetic retinopathy. esRAGE levels in patients with* (n = 24) *and without retinopathy* (n = 43) *were 0.286 ± 0.092 and 0.230 ± 0.074 ng/ml, respectively. There was a significant difference* (P = 0.0124) *in circulating esRAGE levels between the groups.*

tween circulating esRAGE and A1C levels ($r = -0.614$, $P < 0.0001$). Because circulating esRAGE levels also correlated with BMI, DBP, triglyceride levels, and the common logarithm of hs-CRP, we performed a stepwise multivariate regression analysis and found that A1C ($F = 46.1$) and BMI ($F = 9.0$) were independent risk factors for a low esRAGE value. However, whether there is a direct relationship between A1C or BMI and circulating esRAGE levels should be confirmed by further study. It would be necessary to examine the relationship between AGE levels and circulating esRAGE levels before we discuss what factors affect circulating esRAGE levels.

The present study showed that circulating esRAGE levels were inversely correlated with carotid IMT, indicating that esRAGE is inversely correlated with the severity of macroangiopathy. Although carotid IMT is one of the most reliable markers of atherosclerosis, further study using some other indicators of vascular function would be necessary to clarify the relationship between circulating esRAGE levels and macroangiopathy.

The present study also showed that circulating esRAGE levels were significantly lower in subjects with retinopathy than in those without retinopathy (Fig. 2*A*). In addition, our data suggest that circulating esRAGE levels tend to be inversely correlated with daily urinary albumin excretion. However, another

study would be necessary to conclude whether there are some correlations between esRAGE levels and the severity of nephropathy.

It was reported that the C-truncated form of RAGE binds to AGEs and neutralizes their action, leading to vascular dysfunction (11,14,16,17). Furthermore, it was reported that the treatment with C-truncated RAGE stabilizes the progression of atherosclerosis in a mouse model (13,18,22). Taking into account such reports and our present results, it is possible that human circulating esRAGE levels influence the development of diabetic vascular complications. However, further study would be necessary to prove whether diabetic patients with lower circulating esRAGE levels are more susceptible to diabetic vascular diseases.

In summary, circulating esRAGE levels were significantly lower in type 1 diabetic patients than in nondiabetic subjects. The esRAGE levels were inversely correlated with the severity of macroangiopathy and also tended to be inversely correlated with microangiopathy.

References

1. Brownlee M, Cerami A, and Vlassara H: Advanced glycosylation end products in tissue and the biochemical basis of diabetic complications. *N Engl J Med* 318:1315–1321, 1988
2. Schmidt AM, and Stern DM: RAGE: a new target for the prevention and treatment of the vascular and inflammatory complications of diabetes. *Trends Endocrinol Metab* 11:368–375, 2000
3. Stern DM, Yan SD, Yan SF, Schmidt AM: Receptor for advanced glycation endproducts (RAGE) and the complications of diabetes. *Ageing Res Rev* 1:1–15, 2002
4. Sakurai S, Yonekura H, Yamamoto Y, Watanabe T, Tanaka N, Li H, Rahman AK, Myint KM, Kim CH, Yamamoto H: The AGE-RAGE system and diabetic nephropathy. *J Am Soc Nephrol* 14 (Suppl. 3): S259–S263, 2003
5. Naka Y, Bucciarelli LG, Wendt T, Lee LK, Rong LL, Ramasamy R, Yan SF, Schmidt AM: RAGE axis: animal models and novel insights into the vascular complications of diabetes. *Arterioscler Thromb Vasc Biol* 24: 1342–1349, 2004
6. Wautier J-L, Schmidt AM: Protein glycation: a firm link to endothelial cell dysfunction. *Circ Res* 95:233–238, 2004
7. Yamagishi S, Fujimori H, Yonekura H, Yamamoto Y, Yamamoto H: Advanced glycation endproducts inhibit prostacyclin production and induce plasminogen activator inhibitor-1 in human microvascular endothelial cells. *Diabetologia* 41: 1435–1441, 1998
8. Yamagishi S, Hsu C-C, Taniguchi M, Harada S, Yamamoto Y, Ohsawa K, Kobayashi K, Yamamoto H: Receptor-mediated toxicity to pericytes of advanced glycosylation end products: a possible mechanism of pericyte loss in diabetic microangiopathy. *Biochem Biophys Res Commun* 213: 681–687, 1995
9. Yamagishi S, Yamamoto Y, Harada S, Hsu C-C, Yamamoto H: Advanced glycosylation end products stimulate the growth but inhibit the prostacyclin-producing ability of endothelial cells through interactions with their receptors. *FEBS Lett* 384:103–106, 1996
10. Schmidt AM, Hasu M, Popov D, Zhang JH, Chen J, Yan SD, Brett J, Cao R, Kuwabara K, Costache G: Receptor for advanced glycation end products (AGEs) has a central role in vessel wall interactions and gene activation in response to circulating AGE proteins. *Proc Natl Acad Sci U S A* 91:8807–8811, 1994
11. Wautier JL, Zoukourian C, Chappey O, Wautier MP, Guillausseau PJ, Cao R, Hori O, Stern D, Schmidt AM: Receptor-mediated endothelial cell dysfunction in diabetic vasculopathy: soluble receptor for advanced glycation end products blocks hyperpermeability in diabetic rats. *J Clin Invest* 97:238–243, 1996
12. Tsuji H, Iehara N, Masegi T, Imura M, Ohkawa J, Arai H, Ishii K, Kita T, Doi T: Ribozyme targeting of receptor for advanced glycation end products in mouse mesangial cells. *Biochem Biophys Res Commun* 245:583–588, 1998
13. Park L, Raman KG, Lee KJ, Lu Y, Ferran LJ Jr, Chow WS, Stern D, Schmidt AM: Suppression of accelerated diabetic atherosclerosis by the soluble receptor for advanced glycation endproducts. *Nat Med* 4:1025–1031, 1998
14. Schmidt AM, Hori O, Chen JX, Li JF, Crandall J, Zhang J, Cao R, Yan SD, Brett J, Stern D: Advanced glycation endproducts interacting with their endothelial receptor induce expression of vascular cell adhesion molecule-1 (VCAM-1) in cultured human endothelial cells and in mice: a potential mechanism for the accelerated vasculopathy of diabetes. *J Clin Invest* 96: 1395–1403, 1995
15. Neeper M, Schmidt AM, Brett J, Yan SD, Wang F, Pan YC, Elliston K, Stern D, Shaw A: Cloning and expression of a cell surface receptor for advanced glycosylation end products of proteins. *J Biol Chem* 267:14998–15004, 1992
16. Yonekura H, Yamamoto Y, Sakurai S, Petrova RG, Abedin J, Li H, Yasui K, Takeuchi M, Makita M, Takasawa S, Okamoto H, Watanabe T, Yamamoto H: Novel splice variants of the receptor for advanced glycation end-products expressed in human vascular endothelial cells and pericytes, and their putative roles in diabetes-induced vascular injury. *Biochem J* 370:1097–1109, 2003
17. Yonekura H, Yamamoto Y, Sakurai S, Watanabe T, Yamamoto H: Roles of the receptor for advanced glycation endproducts in diabetes-induced vascular injury. *J Pharmacol Sci* 97:305–311, 2005
18. Bucciarelli LG, Wendt T, Qu W, Lu Y, Lalla E, Rong LL, Goova MT, Moser B, Kislinger T, Lee DC, Kashyap Y, Stern DM, Schmidt AM: RAGE blockade stabilizes established atherosclerosis in diabetic apolipoprotein E-null mice. *Circulation* 206:2827–2835, 2002
19. Yamasaki Y, Kawamori R, Matsushima H, Nishizawa H, Kodama M, Kajimoto Y, Morishima T, Kamada T: Atherosclerosis in carotid artery of young IDDM patients monitored by ultrasound high-resolution B-mode imaging. *Diabetes* 43:634–639, 1994
20. Kawamori R, Yamasaki Y, Matsushima H, Nishizawa H, Nao K, Hougaku H, Maeda H, Handa N, Matsumoto M, Kamada T: Prevalence of carotid atherosclerosis in diabetic patients: ultrasound high-resolution B-mode imaging on carotid arteries. *Diabetes Care* 15:1290–1294, 1992
21. Pignoli P, Tremoli E, Poli A, Oreste P, Paoletti R: Intimal plus medial thickness of the arterial wall: a direct measurement with ultrasound imaging. *Circulation* 74: 1399–1406, 1986
22. Sakaguchi T, Yan SF, Yan SD, Belov D, Rong LL, Sousa M, Andrassy M, Marso SP, Duda S, Arnold B, Liliensiek B, Nawroth PP, Stern DM, Schmidt AM, Naka Y: Central role of RAGE-dependent neointimal expansion in arterial restenosis. *J Clin Invest* 111:959–972, 2003

PDX-1/VP16 Fusion Protein, Together With NeuroD or Ngn3, Markedly Induces Insulin Gene Transcription and Ameliorates Glucose Tolerance

Hideaki Kaneto, Yoshihisa Nakatani, Takeshi Miyatsuka, Taka-aki Matsuoka, Munehide Matsuhisa, Masatsugu Hori, and Yoshimitsu Yamasaki

Diabetes is the most prevalent and serious metabolic disease, and the number of diabetic patients worldwide is increasing. The reduction of insulin biosynthesis in pancreatic β-cells is closely associated with the onset and progression of diabetes, and thus it is important to search for ways to induce insulin-producing cells in non−β-cells. In this study, we showed that a modified form of the pancreatic and duodenal homeobox factor 1 (PDX-1) carrying the VP16 transcriptional activation domain (PDX-1/VP16) markedly increases insulin biosynthesis and induces various pancreas-related factors in the liver, especially in the presence of NeuroD or neurogenin 3 (Ngn3). Furthermore, in streptozotocin-induced diabetic mice, PDX-1/VP16 overexpression, together with NeuroD or Ngn3, drastically ameliorated glucose tolerance. Thus PDX-1/VP16 expression, together with NeuroD or Ngn3, markedly induces insulin gene transcription and ameliorates glucose tolerance. This approach warrants further investigation and may have utility in the treatment of diabetes. *Diabetes* 54: 1009–1022, 2005

The pancreatic and duodenal homeobox factor 1 (PDX-1), a member of the homeodomain-containing transcription factor family (also known as IDX-1/STF-1/IPF1) (1–3), is expressed in the pancreas and duodenum and plays a crucial role in pancreas development (4–14), β-cell differentiation (15–26), and maintenance of normal β-cell function by regulating several β-cell−related genes (14,27–37). At early stages of embryonic development, PDX-1 is initially expressed in the gut region when the foregut endoderm becomes committed to common pancreatic precursor cells (1,4–7,11,13). During pancreas development, PDX-1 expression is maintained in precursor cells that coexpress several hormones; later, its expression is restricted to β-cells (1–3,5,6,11,13,28). Mice homozygous for a targeted mutation in the PDX-1 gene are apancreatic and develop fatal perinatal hyperglycemia (4), and heterozygous PDX-1−deficient mice have impaired glucose tolerance (12); both of these findings suggest the crucial role PDX-1 plays in pancreas development. In clinical manifestations, mutations in PDX-1 are known to cause maturity-onset diabetes of the young (MODY) (38).

NeuroD, a member of the basic helix-loop-helix (bHLH) transcription factor family, also known as BETA2, is expressed in pancreatic and intestinal endocrine cells and neural tissue. NeuroD also plays an important role in pancreas development and the regulation of insulin gene transcription (39–41). It has been reported that the insulin-enhancer elements E-box and A-box play an important role in regulating cell-specific expression of the insulin gene (42,43), and that NeuroD's binding to the E-box as well as PDX-1's binding to the A-box are very important for insulin gene transcription. Mice homozygous for the null mutation in NeuroD have a striking reduction in the number of β-cells, develop severe diabetes, and die perinatally (40). In clinical manifestations, mutations in NeuroD cause MODY (44). Neurogenin 3 (Ngn3) is also a bHLH transcription factor that binds to the E-box and is involved in pancreas development (45–50). Transgenic mice overexpressing Ngn3 early in their development show a marked increase in endocrine cell formation, indicating that Ngn3 induces differentiation of islet cell precursors (46,47). In contrast, mice with targeted disruption of Ngn3 have no endocrine cells (48).

Insulin plays a crucial role in maintaining blood glucose levels; insulin facilitates glucose uptake into muscle and adipose tissue and suppresses gluconeogenesis in the liver. In addition, insulin signaling has a functional role in β-cells themselves; it has been reported that insulin signaling is crucial for insulin gene expression and glucose-stimulated insulin secretion (49–52). In the diabetic state, however, hyperglycemia (53–60) and subsequent production of reactive oxygen species (61–65) decrease insulin gene expression and secretion, accompanied by reduced PDX-1 expression and DNA binding activity. Although pancreas and islet transplantation efficiently restore normoglycemia, such treatment requires lifelong immunosup-

From the Department of Internal Medicine and Therapeutics, Osaka University Graduate School of Medicine, Osaka, Japan.

Address correspondence and reprint requests to Hideaki Kaneto, MD, PhD, Department of Internal Medicine and Therapeutics, Osaka University Graduate School of Medicine, 2-2 Yamadaoka, Suita, Osaka 565-0871, Japan. E-mail: kaneto@medone.med.osaka-u.ac.jp.

Received for publication 28 July 2004 and accepted in revised form 7 January 2005.

H.K. and Y.N. contributed equally to this work.

ABC, avidin-biotin complex; Ad, adenovirus; ALT, alanine aminotransferase; AST, aspartic acid aminotransferase; bHLH, basic helix-loop-helix; DAB, 3, 3′-diaminobenzidine tetrahydrochloride; GFP, green fluorescent protein; MODY, maturity-onset diabetes of the young; Ngn3, neurogenin 3; PDX-1, pancreatic and duodenal homeobox factor 1; PFU, plaque forming unit; STZ, streptozotocin; TBS, Tris-buffered saline.

pressive therapy and is limited by tissue supply (66,67). Therefore, it is important to search for ways to enhance insulin gene transcription and induce insulin-producing cells. Although the pancreas and liver arise from adjacent regions of the endoderm in embryonic development, the liver is a potential target for diabetes gene therapy (16,19,41,68–73). Moreover, it has been shown recently that a modified form of XlHbox8, the *Xenopus* homolog of PDX-1, carrying the VP16 transcriptional activation domain from the herpes simplex virus, efficiently induces insulin gene expression in the liver of the tadpole (72,73). Thus, although PDX-1 expression itself is obviously important, as has been demonstrated by various studies, it is likely that PDX-1 requires the recruitment of coordinately functioning transcription factors or cofactors to fully exert its function.

In this study, we showed that PDX-1/VP16 expression, together with NeuroD or Ngn3, markedly induces insulin gene transcription and ameliorates glucose tolerance in diabetic animals, implying that this combination is useful for replacing the reduced β-cell function found in diabetes.

RESEARCH DESIGN AND METHODS

Gene transfection and luciferase assays. HepG2 cells were grown in Eagle's minimum essential medium supplemented with 10% FCS, 100 units/ml penicillin, and 0.1 mg/ml streptomycin sulfate in a humidified atmosphere of 5% CO_2 at 37°C. The insulin 2 promoter-reporter (firefly luciferase) plasmid (1.0 μg) containing 5′-flanking sequences of the rat insulin 2 promoter region (−238 bp to 3 bp) (42,74) and 0.5 μg of the pSV−β-galactosidase control vector (Promega) were cotransfected with 1.0 μg of the PDX-1, PDX-1/VP16 , NeuroD, and/or Ngn3 expression plasmids (or empty vectors) using LipofectAMINE reagent (Life Technologies). The insulin 2 promoter-reporter (firefly luciferase) plasmid containing A3-box− or E1-box−mutated 5′-flanking sequences of the rat insulin 2 promoter region (−238 bp to 3 bp) (42,74) was similarly transfected. The A3-box is the most important PDX-1 binding site for insulin gene transcription, and the rat insulin 2 promoter has only one E-box to which NeuroD is known to bind. The PDX-1/VP16 (amino acid 410–490) fusion plasmid was made by PCR using the VP16 plasmid (kindly provided by Dr. Daniel S. Kessler, University of Pennsylvania School of Medicine) and rat PDX-1 expression plasmid as templates; the resulting clones were verified by sequencing. Cells were harvested for luciferase and β-galactosidase assays 48 h after transfection. Preparations of cellular extracts were assayed using a luciferase assay system (Promega). For the luciferase assay, light emission was measured with a Monolight 3010 Luminometer (Pharmingen, San Diego, CA), and β-galactosidase assays were performed with the β-galactosidase enzyme assay system (Promega). The luciferase results were normalized with respect to transfection efficiency as assessed from the results of the β-galactosidase assays.

Preparation of recombinant adenoviruses expressing PDX-1, PDX-1/VP16, NeuroD, and Ngn3. Recombinant adenoviruses expressing PDX-1, PDX-1/VP16 , NeuroD, and Ngn3 were prepared using the AdEasy system (kindly provided by Dr. Bert Vogelstein, Johns Hopkins Oncology Center) (75). In brief, the encoding region of PDX-1, PDX-1/VP16 , NeuroD, and Ngn3 was cloned into a shuttle vector pAdTrack-CMV. To produce an homologous recombination, 1.0 μg of linearized plasmid containing PDX-1, PDX-1/VP16 , NeuroD, or Ngn3 and 0.1 μg of the adenoviral backbone plasmid pAdEasy-1 were introduced into electrocompetent *E. coli* BJ5183 cells by electroporation (2,500 V, 200 Ohms, 25 μFD). The resultant plasmids were then retransformed into *E. coli* XL-Gold Ultracompetent Cells (Stratagene, La Jolla, CA). The plasmids were linearized with *Pac* I and then transfected into the adenovirus packaging cell line 293 using LipofectAMINE (Invitrogen, Carlsbad, CA). The cell lysate was collected from 293 cells 10 days after transfection and added to a fresh batch of 293 cells. When most of the cells were killed by the adenovirus infection and detached, the cell lysate was obtained. This process was repeated three times. The control adenovirus expressing green fluorescent protein (Ad-GFP) was prepared in the same manner. The adenovirus titers were further increased up to 1×10^{10} plaque forming units (PFU)/ml using the Adeno-X Virus Purification Kit (Clontech). The virus titers were estimated using the Adeno-X Titer Kit (Clontech).

Induction of hyperglycemia by streptozotocin and treatment with recombinant adenovirus. C57BL/6 male mice (age 8 weeks; Japan SLC, Hamamatsu, Japan) were made diabetic by streptozotocin injection (STZ; 220 mg/kg, i.p.; Sigma) freshly dissolved in citrate buffer (pH 4.5). Mice were injected with 100 μl of Ad–PDX-1, Ad–PDX-1/VP16, Ad-NeuroD, Ad-Ngn3, or Ad-GFP (1×10^{10} PFU/ml) into the cervical vein 1 week after STZ injection. We adjusted the total volume of the injected adenovirus; for example, when PDX-1 (100 μl) was combined with NeuroD or Ngn3 (100 μl), the PDX-1 alone control consisted of PDX-1 (100 μl) and GFP (100 μl). Although it is easier to inject the adenovirus via the tail vein rather than the cervical vein, in our experiments we injected the adenovirus via the cervical vein to ensure there was no leakage during the injection. After the adenovirus injection, nonfasting blood glucose levels were measured regularly with a portable glucose meter (Precision QID; Medisense, St. Charles, MA) after snipping the tail. To measure plasma insulin levels, nonfasting blood samples were collected into heparinized capillary tubes and plasma insulin levels were determined using an Insulin-EIA Test Kit (Glazyme).

Glucose tolerance tests. After being fasted overnight, mice were injected with glucose (1.0 g/kg body wt, i.p.). Blood samples were taken at various time points (0–120 min), and blood glucose levels were determined as described above.

RT-PCR analysis. Total RNA was extracted from frozen tissues using Trizol (Invitrogen). After quantifying RNA by spectrophotometry, 2.5 μg of RNA were heated at 85°C for 3 min and then reverse-transcribed into cDNA in a 25-μl solution containing 200 units of Superscript II RNase H-RT (Invitrogen), 50 ng random hexamers (Invitrogen), 160 μmol/l dNTP, and 10 mmol/l dithiothreitol. The reaction consisted of 10 min at 25°C, 60 min at 42°C, and 10 min at 95°C. Polymerization reactions were performed with a PerkinElmer 9700 Thermocycler (Norwalk, CT) using a 50-μl reaction volume containing 3 μl of cDNA (20 ng RNA equivalents), 5 units of AmpliTaq Gold DNA polymerase (PerkinElmer), 1.5 mmol/l MgCl2, 160 μmol/l cold dNTPs, and 10 pmol of appropriate oligonucleotide primers. The oligonucleotide primers were as follows: insulin 1 (370 bp), GAC CAG CTA TAA TCA GAG ACC (forward), AGT TGC AGT AGT TCT CCA GCT G (reverse); insulin 2 (388 bp), AGC CCT AAG TGA TCC GCT ACA A (forward), AGT TGC AGT AGT TCT CCA GCT G (reverse); glucokinase (islet type; 208 bp), TGG ATG ACA GAG CCA GGA TGG (forward), ACT TCT GAG CCT TCT GGG GTG (reverse); SUR-1 (267 bp), CCA GAC CAA GGG AAG ATT CA (forward), GTC CTG TAG GAT GAT GGA CA (reverse); Kir6.2 (218 bp), CCT GAG GAA TAT GTG CTG AC (forward), CAC AGG AAG GAC ATG GTG AA, (reverse); glucagon (205 bp), ACA GAG GAG AAC CCC AGA TC (forward), CAT CAT GAC GTT TGG CAA TG (reverse); somatostatin (226 bp), AGT TTC TGC AGA AGT CTC TGG (forward), AAG TTC TTG CAG CCA GCT TTG (reverse); and pancreatic polypeptide (194 bp), ACA GGA TGG CCG TCG CAT ACT (forward), GGC CTG GTC AGT GTG TTG ATG (reverse). The thermal cycle profile used a 10-min denaturing step at 94°C followed by 32 cycles (1 min of denaturation at 94°C, 1 min of annealing at 55°C, and 1 min of extension at 72°C) and an extension step of 10 min at 72°C. The products were then separated by agarose gel electrophoresis.

Northern blot analysis. Total RNA (10 μg) isolated from freeze-clamped liver tissues were electrophoresed on 1.0% formaldehyde-denatured agarose gel in 1 × MOPS running buffer, and then transferred overnight to a Hybond-N^+ membrane (Amersham, Arlington Heights, IL). The insulin probe was labeled with [α-^{32}P]dCTP using the Rediprime labeling system kit (Amersham). After being hybridized overnight with a ^{32}P-labeled probe at 42°C, the membranes were washed in 2 × sodium chloride−sodium phosphate EDTA buffer, 0.1% SDS at 42°C. Kodak XAR film was exposed with an intensifying screen at −80°C.

Western blot analysis. Whole-cell extracts obtained from various tissues were fractionated by 10% SDS-PAGE and transferred to reinforced cellulose nitrate membrane (Optitran BA-S85; Schleicher & Schuell). After blocking, the membranes were incubated at 4°C overnight in Tris-buffered saline (TBS; 50 mmol/l Tris-HCl, 150 mmol/l NaCl) containing a 1:500 dilution of GFP antibody (Living Colors AV peptide antibody; Clontech) and then incubated for 1 h at room temperature in TBS containing a 1:1,000 dilution of anti-rabbit IgG antibody coupled to horseradish peroxidase (Bio-Rad). Immunoreactive bands were visualized by incubation with LumiGLO (Cell Signaling) and exposure to light-sensitive film.

Immunohistochemical analyses. The mice were anesthetized using sodium pentobarbital. After a midline abdominal incision was made, liver tissues were removed from the mice and fixed overnight with 4% paraformaldehyde in PBS buffer. Fixed tissues were routinely processed for paraffin embedding and ~4-μm sections were prepared and mounted on slides. Before being incubated with antibodies, the mounted sections were rinsed three times with PBS. To detect PDX-1, NeuroD, and Ngn3, the avidin-biotin complex (ABC) method was performed using the Vectastain ABC Kit (Vector Laboratories,

Burlingame, CA). After being treated with Target Retrieval Solution (Dako) at 90°C for 5 min, the mounted sections were incubated overnight with rabbit anti–PDX-1 antiserum (30), goat anti-NeuroD antibody (N-19; Santa Cruz), and goat anti-Ngn3 antibody (D-15; Santa Cruz) diluted 1:1,000 in PBS containing 1% BSA. This was followed by a 1-h incubation with biotinylated anti-rabbit IgG (for PDX-1) or anti-goat IgG (for NeuroD and Ngn3) (Vector Laboratories) diluted 1:200. The sections were then incubated with ABC reagent for 1 h, and positive reactions were visualized by incubation with the peroxidase substrate solution containing 3,3′-diaminobenzidine tetrahydrochloride (DAB; Zymed Laboratories, San Francisco, CA). To detect insulin, the mounted sections were incubated overnight with guinea pig polyclonal anti-insulin antibody (Dako, Glostrup, Denmark) diluted 1:1,000 in PBS containing 1% BSA and then incubated for 1 h at room temperature with goat anti–guinea pig IgG (1:200; Alexa 546; Molecular Probes). To detect C-peptide, the ABC method was performed using a Vectastain ABC Kit. The mounted sections were incubated overnight with goat anti–C-peptide antiserum (Linco Research, St. Charles, MO) diluted 1:100 in PBS containing 1% BSA. This was followed by a 1-h incubation with biotinylated anti-goat IgG diluted 1:200. The sections were then incubated with ABC reagent for 1 h, and positive reactions were visualized by incubation with the peroxidase substrate solution containing DAB.

Electron microscopy. Liver tissues were fixed with 2% OsO_4 at 4°C for 2 h. After being dehydrated with ascending concentrations of ethanol, the tissues were embedded in Quetol 812 resin. Ultra-thin sections (80–90 nm) mounted on copper grids were stained with aqueous uranyl acetate for 15 min and Reynolds' lead citrate for 5 and 3 min, respectively, then viewed using a Hitachi H-300 electron microscope.

RESULTS

Adenovirus-mediated expression of PDX-1, NeuroD, and Ngn3 induces insulin gene expression in the liver and ameliorates glucose tolerance in diabetic animals. To evaluate the possible effect of ectopic expression of PDX-1, NeuroD, and Ngn3 in the liver, we prepared PDX-1–, NeuroD-, and Ngn3-expressing adenoviruses (Ad–PDX-1, Ad-NeuroD, and Ad-Ngn3) and a control adenovirus (Ad-GFP) and delivered each adenovirus to 8-week-old male C57BL/6 mice. Figure 1*A* (*upper panel*) shows a representative liver after exposure to the adenovirus. As seen by GFP in this fluorescent micrograph of a liver, many cells were infected with the adenovirus. To confirm that infected adenoviruses can express the target proteins in the liver, we performed immunostaining for PDX-1, NeuroD, and Ngn3. As shown in Fig. 1*A* (*middle panels*), PDX-1, NeuroD, and Ngn3 were clearly detected in the liver after infection with Ad–PDX-1, Ad-NeuroD, and Ad-Ngn3, respectively. These three transcription factors were not detected at all in the liver without each adenovirus infection or by an immunostaining without each primary antibody (data not shown). In addition, it is known that PDX-1 and NeuroD are expressed in mature pancreatic islets and that Ngn3 is transiently expressed at the embryonic stage during pancreas development. As expected, PDX-1 and NeuroD, but not Ngn3, were clearly detected in mouse mature pancreatic islets by immunostaining using the same antibodies (Fig. 1*A*, *lower panels*). To confirm that the adenovirus was infected only in the liver, we examined GFP expression in various tissues (brain, heart, lung, liver, spleen, pancreas, kidney, fat, and muscle). As shown in Fig. 1*B*, GFP was expressed in the liver, but not in any other tissues, indicating that the adenovirus was infected only in the liver. In addition, after injection of each adenovirus, we examined the expression of PDX-1, NeuroD, and Ngn3 in various tissues. Without the adenovirus injection, PDX-1 and NeuroD were detected only in the pancreas (endogenous PDX-1 and NeuroD were detected) and Ngn3 was not detected in any tissue. After each adenovirus injection, expression of these three transcription factors was increased only in the liver, but not in any other tissues, indicating that the adenoviruses were infected only in the liver (data not shown).

Insulin 2 gene expression was detected 3 days after the injection of Ad–PDX-1 (Fig. 2*A*), whereas insulin 1 gene expression was not detected at all (data not shown). Similar results were obtained after treatment with Ad-NeuroD or Ad-Ngn3. Also, larger amounts of insulin 2 gene expression were detected in the liver 3 days after the infection of Ad–PDX-1 plus Ad-NeuroD or Ad-Ngn3. Insulin 2 gene expression was still detected 14 days after adenovirus injection, although expression levels were slightly attenuated. In addition, we thought that insulin production in the liver might be easily induced by such transcription factors when pancreatic β-cells are destroyed and/or blood glucose levels are high. To examine this possibility, we compared the induction of insulin mRNA expression in nondiabetic C57BL/6 mice and STZ-induced diabetic mice. However, there was no difference in the induction of insulin mRNA expression by such transcription factors between nondiabetic C57BL/6 mice (Fig. 2*A*) and STZ-induced diabetic mice (Fig. 2*B*).

To examine whether hepatic insulin production induced by PDX-1, NeuroD, and/or Ngn3 is capable of controlling blood glucose levels in diabetic mice, we injected 220 mg/kg STZ into C57BL/6 mice and 1 week later treated the mice with Ad–PDX-1, Ad-NeuroD, Ad-Ngn3, or control Ad-GFP. When PDX-1 was ectopically induced in the liver, insulin 2 gene expression was clearly observed (Fig. 2*B*), whereas insulin 1 gene expression was not detected at all (data not shown). In addition, larger amounts of insulin 2 gene expression were induced in the liver by the overexpression of PDX-1 plus NeuroD or Ngn3. Furthermore, 3 days after adenovirus injection, blood glucose levels were moderately decreased by PDX-1 alone (Fig. 3*A*) and more significantly decreased by overexpression of PDX-1 plus NeuroD or Ngn3 (Fig. 3*B*). After that, however, blood glucose levels gradually increased.

Overexpression of a modified form of PDX-1 carrying the VP16 transcriptional activation domain, together with NeuroD or Ngn3, markedly increases insulin gene promoter activity in HepG2 cells and is more effective than wild-type PDX-1. It has been shown recently that a modified form of XlHbox8, the *Xenopus* homolog of PDX-1 carrying the VP16 transcriptional activation domain from herpes simplex virus, efficiently induces insulin gene expression in the liver (72,73). To evaluate the effect of PDX-1, PDX-1/VP16, NeuroD, and Ngn3 expression on insulin gene transcription, we examined insulin gene promoter activity in HepG2 cells after transient transfection of each expression plasmid. As shown in Fig. 4*A*, basal insulin promoter activity was very low in HepG2 cells but moderately increased after the transfection of PDX-1, NeuroD, or Ngn3 and was more clearly increased by overexpression of PDX-1 plus NeuroD or Ngn3. Also, although PDX-1/VP16 exerted only a slightly more obvious effect on the insulin promoter compared with wild-type PDX-1, PDX-1/VP16 together with NeuroD or Ngn3 dramatically increased insulin promoter activity (nearly 300-fold increase).

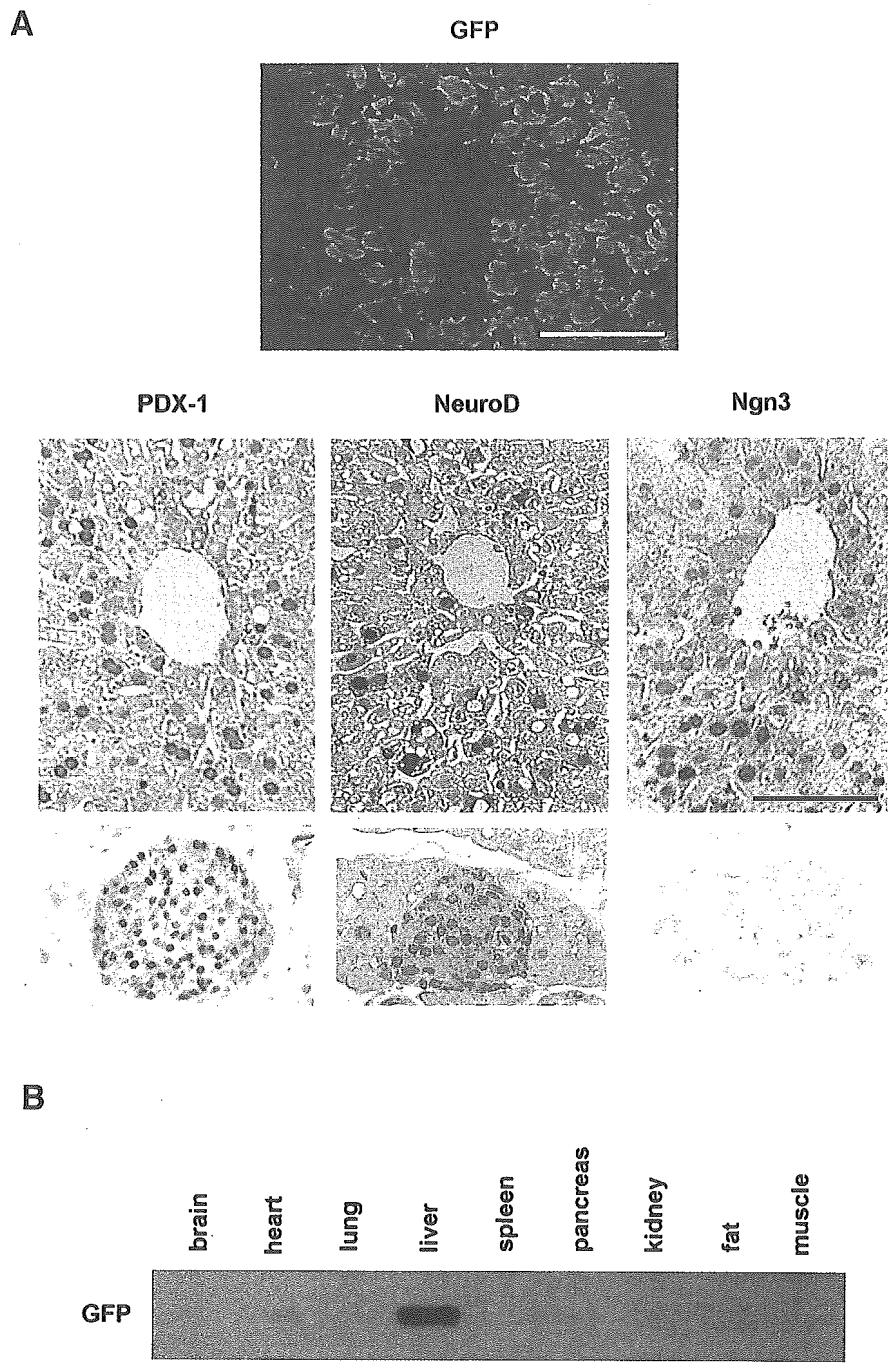

FIG. 1. Adenovirus-mediated expression of PDX-1, NeuroD, and Ngn3 in the liver. *A*: Male C57BL/6 mice were injected with Ad–PDX-1, Ad-NeuroD, Ad-Ngn3, or Ad-GFP (1×10^{10} PFU/ml) into the cervical vein. Each panel shows a representative liver after exposure to each adenovirus. As seen with GFP (*upper panel*), many cells in the liver were infected after exposure to Ad-GFP. PDX-1, NeuroD, or Ngn3 protein expression was also clearly detected in the liver after infection with Ad-PDX, Ad-NeuroD, or Ad-Ngn3 (*middle panels*). Bar, 50 μm. In addition, it is known that PDX-1 and NeuroD are expressed in mature pancreatic islets and that Ngn3 is transiently expressed at the embryonic stage during pancreas development. As expected, PDX-1 and NeuroD, but not Ngn3, were clearly detected in mouse mature pancreatic islets by immunostaining using the same antibodies (*lower panels*). *B*: Male C57BL/6 mice were injected with Ad-GFP into the cervical vein. We then obtained whole cell extracts from various tissues (brain, heart, lung, liver, spleen, pancreas, kidney, fat, and muscle) and performed Western blot analysis with anti-GFP antibody.

In addition, A3-box– and E1-box–mutated insulin promoter activities were also increased by overexpression of PDX-1/VP16 plus NeuroD or Ngn3, but the extent of the increase was much less obvious compared with their effects on wild-type insulin promoter activity (Fig. 4*B*). The A3-box is the most important PDX-1 binding site for insulin gene transcription, and the rat insulin 2 promoter has only one E-box to which NeuroD is known to bind. These results suggest that PDX-1/VP16 plus NeuroD or Ngn3 exerts synergistic effects on insulin gene transcription in an A-box– and E-box–dependent manner.

Adenoviral PDX-1/VP16 expression, together with NeuroD or Ngn3, markedly induces insulin and other various pancreas-related factors. To examine the additional effect of VP16 on PDX-1–mediated induction of insulin gene expression, we prepared an adenovirus expressing the PDX-1/VP16 fusion protein (Ad–PDX-1/VP16) and delivered the adenovirus to 8-week-old male C57BL/6 mice. As shown in Fig. 5*A*, 3 days after Ad–PDX-1/VP16 injection, insulin 1 and 2 were both detected by RT-PCR, although insulin 1 was not detected by the expression of wild-type PDX-1 in the absence of VP16. In addition, larger

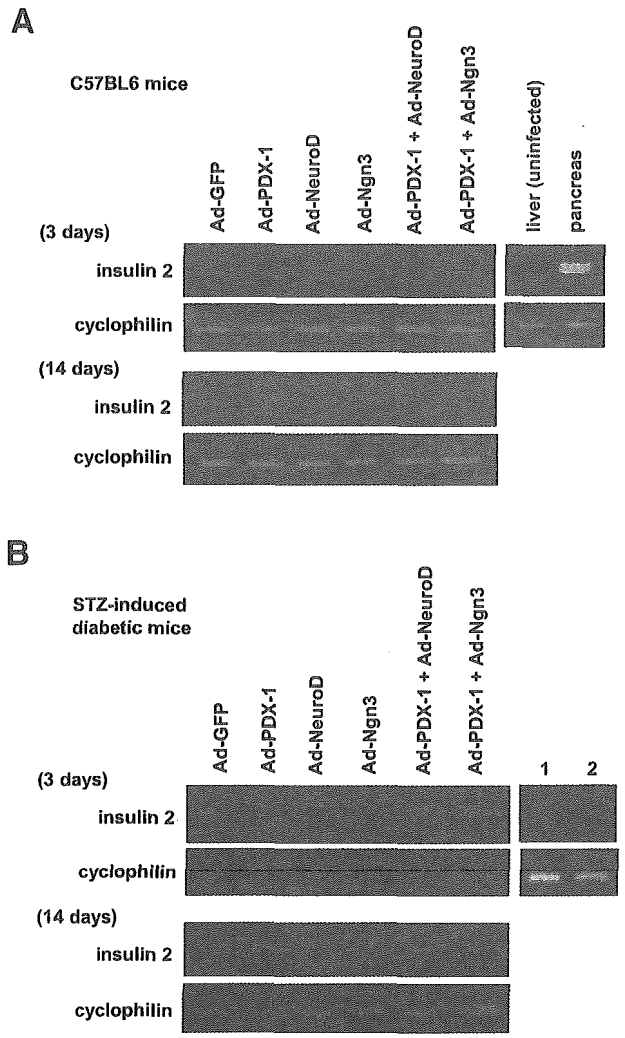

FIG. 2. Adenoviral expression of PDX-1, NeuroD, and Ngn3 in the liver induces insulin gene expression. *A*: Male C57BL/6 mice were injected with Ad–PDX-1, Ad-NeuroD, Ad-Ngn3, or Ad-GFP (1×10^{10} PFU/ml). Then, 3 (*upper panel*) and 14 (*lower panel*) days after the injection we examined insulin mRNA expression by RT-PCR. Insulin mRNA expression in the liver and pancreas without adenovirus treatment is also shown (*right panel*). *B*: Male C57BL/6 mice were made diabetic with STZ and injected with Ad–PDX-1, Ad-NeuroD, Ad-Ngn3, or Ad-GFP (1×10^{10} PFU/ml) 1 week later. Then 3 (*upper panel*) and 14 (*lower panel*) days after injection, we examined insulin mRNA expression by RT-PCR. Similar results were obtained in three independent experiments. Insulin mRNA expression in the liver (*lane 1*) and pancreas (*lane 2*) after STZ administration are also shown (*right panel*).

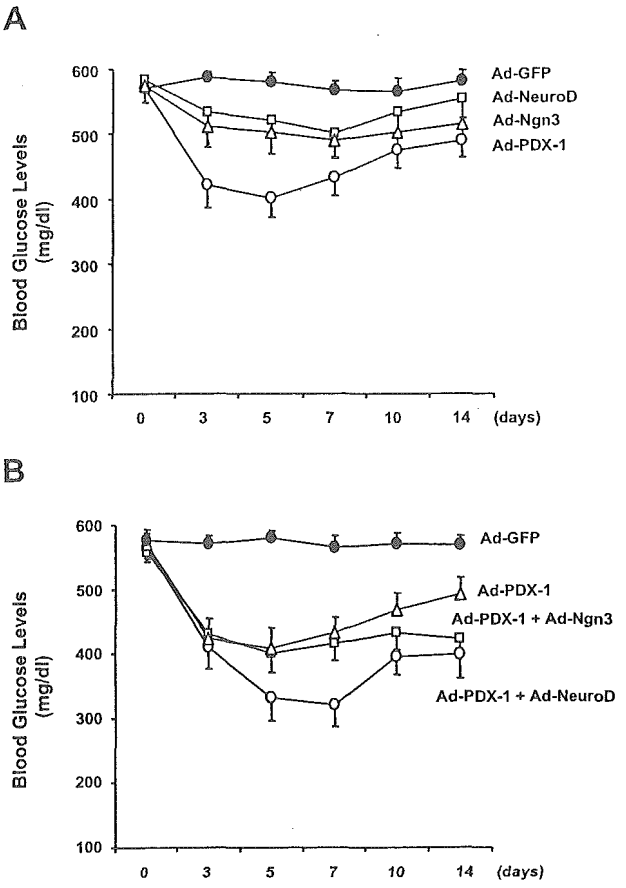

FIG. 3. Adenoviral PDX-1 expression in the liver, together with NeuroD or Ngn3, decreases blood glucose levels in diabetic animals. Male C57BL/6 mice were made diabetic with STZ and 1 week later infected with Ad–PDX-1, Ad-NeuroD, Ad-Ngn3, or Ad-GFP (*A*) and Ad–PDX-1 plus Ad-NeuroD or Ad-Ngn3 (*B*) (1×10^{10} PFU/ml). Nonfasting blood glucose levels were measured with a portable glucose meter after tail snipping. Data are means ± SE ($n = 6$).

amounts of insulin gene expression were detected by PDX-1/VP16 in the presence of NeuroD or Ngn3. The expression of insulin 1 and 2 mRNA could still be clearly detected 14 days after the adenovirus injection. Similar results were obtained when STZ-induced diabetic mice were treated with Ad–PDX-1/VP16 in the absence or presence of Ad-NeuroD or Ad-Ngn3 (Fig. 5*B*). We further evaluated insulin mRNA levels by Northern blot analysis. Insulin mRNA was detected 3 (Fig. 6*A*, *lane 7*) and 14 (Fig. 6*B*) days after Ad–PDX-1/VP16 injection. In addition, larger amounts of insulin gene expression were detected by treatment with Ad–PDX-1/VP16 plus Ad-NeuroD (*lane 7*) or with Ad-Ngn3 (*lane 9*). After treatment with Ad–PDX-1 plus Ad-NeuroD (*lane 5*) or Ad-Ngn3 (*lane 6*), insulin mRNA was also detected by Northern blot analysis, although insulin mRNA was not detected by Ad–PDX-1, Ad-NeuroD, or Ad-Ngn3 alone (*lanes 2–4*)

To examine whether insulin protein was synthesized and stored in the liver, we examined insulin protein expression in the liver after treatment with the adenoviruses. As shown in Fig. 7*A* (*upper panel*), immunostaining for insulin 3 days after treatment with Ad–PDX-1/VP16 plus Ad-NeuroD revealed several insulin-positive cells in cytoplasm (*arrows*; *red cells*). Insulin was not detected at all in the control liver (*middle panel*) or by immunostaining without primary antibody (*lower panel*). Similarly, several insulin-positive cells were observed after treatment with Ad–PDX-1/VP16 plus Ad-Ngn3 (data not shown).

To examine insulin processing, we performed immunostaining for C-peptide. As shown in Fig. 7*B*, C-peptide was clearly detected in the liver after treatment with Ad–PDX-1/VP16 plus Ad-NeuroD (*arrows*; *brown cells*). Similarly, C-peptide–positive cells were observed in the liver after treatment with Ad–PDX-1/VP16 plus Ad-Ngn3 but were not detected at all in the control liver or by immunostaining

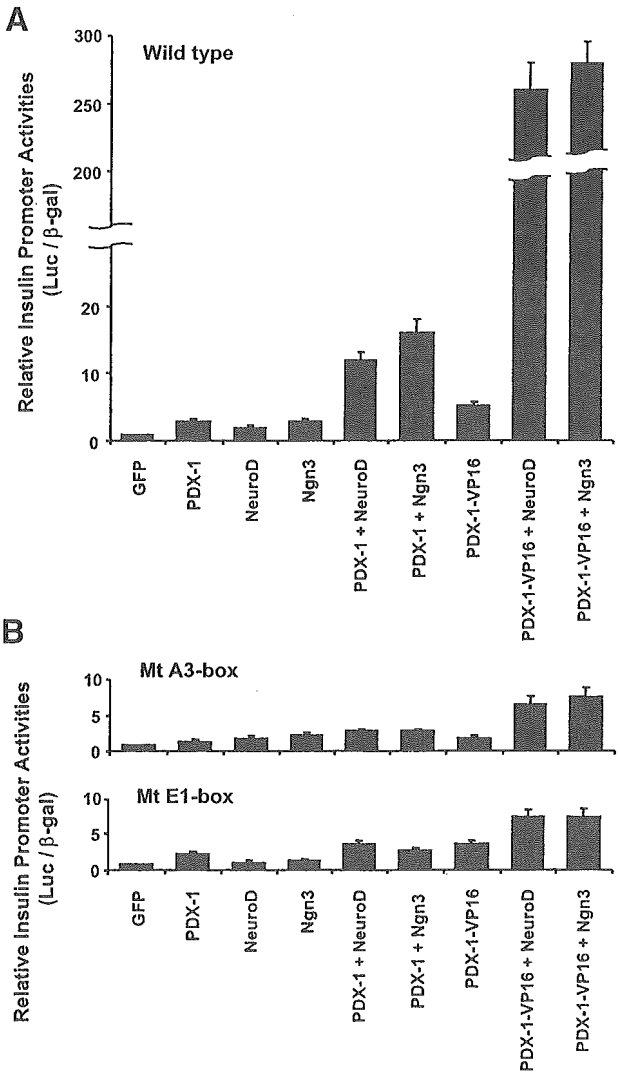

FIG. 4. PDX-1/VP16 expression, together with NeuroD or Ngn3, markedly increases insulin gene promoter activity in HepG2 cells. *A*: The rat insulin promoter-reporter (luciferase; Luc) plasmid and pSV-β-galactosidase control vector (β-gal) were cotransfected into HepG2 cells with the PDX-1, PDX-1/VP16, NeuroD, and/or Ngn3 expression plasmids (or empty vector). After 48 h, luciferase and β-galactosidase assays were performed. *B*: The A3-box– or E1-box–mutated rat insulin promoter-reporter plasmid and the pSV–β-galactosidase control vector were cotransfected into HepG2 cells with the PDX-1, PDX-1/VP16, NeuroD, and/or Ngn3 expression plasmids (or empty vector). After 48 h, luciferase and β-galactosidase assays were performed. The luciferase results were normalized with respect to the transfection efficiency assessed from the results of the β-galactosidase assays. Data are means ± SE, with the basal insulin promoter activity being arbitrarily set at 1 (n = 4).

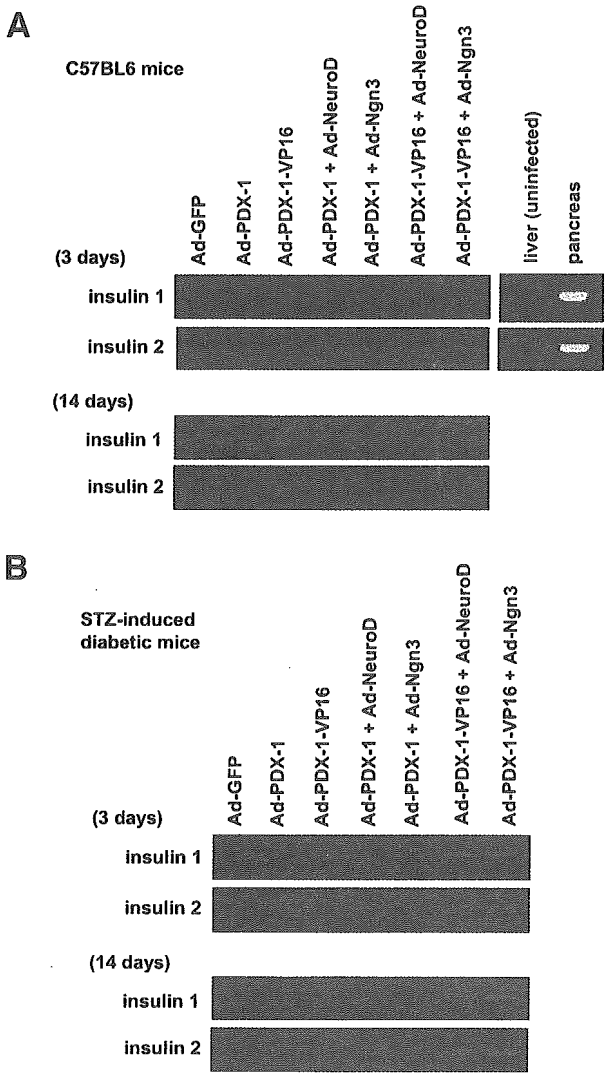

FIG. 5. Adenoviral expression of PDX-1/VP16 in the liver, together with NeuroD or Ngn3, induces insulin gene expression. *A*: Male C57BL/6 mice were injected with Ad–PDX-1, Ad-NeuroD, Ad-Ngn3, or Ad-GFP (1×10^{10} PFU/ml) into the cervical vein. Then, 3 (*upper panel*) and 14 (*lower panel*) days after the injection we examined insulin 1 and 2 mRNA expression by RT-PCR. Insulin mRNA expression in the liver and pancreas without the adenovirus treatment is also shown (*right panel*). *B*: Male C57BL/6 mice were made diabetic with STZ and 1 week later were injected with Ad–PDX-1/VP16, Ad-NeuroD, Ad-Ngn3, or Ad-GFP (1×10^{10} PFU/ml). Then 3 (*upper panel*) and 14 (*lower panel*) days after the injection, we examined insulin 1 and 2 mRNA expression by RT-PCR. Similar results were obtained in three independent experiments.

without primary antibody (data not shown). Although many cells in the liver were infected with the adenovirus, all cells did not necessarily express substantial amounts of insulin; ~3 of 100 cells in the liver started expressing substantial amounts of insulin in the liver. To further evaluate insulin biosynthesis in the liver, we performed electron microscopy. As shown in Fig. 7*C*, several insulin secretory granule–like granules (*arrows in left upper and lower panels*) were observed in the liver after treatment with Ad–PDX-1/VP16 plus Ad-NeuroD, although these were not observed in the control liver (*right panel*). These granules had the typical crystal-like structure inside (*left upper panel*), which is characteristic of insulin secretory granules. In addition, it is known that insulin secretory granules are often withdrawn into their vesicles. As shown in Fig. 7*C* (*left lower panel*), several granules were withdrawn into their vesicles. Peroxisome was observed even in control liver (*arrow heads in right panel*) but was different from insulin secretory granules. In this study, we did not examine the secretory granules in detail, and thus the morphology of the granules is not conclusive. How-